Precambrian Research 377 (2022) 106699

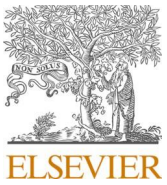

Contents lists available at ScienceDirect

Precambrian Research

journal homepage: www.elsevier.com/locate/precamres

Integrated study of the Doushantuo Formation in northwestern Hunan Province: Implications for Ediacaran chemostratigraphy and biostratigraphy in South China

Hongyi Shi [a,b], Qing Ouyang [a,c,*], Chuanming Zhou [a,b], Shuhai Xiao [d], Zhe Chen [a,b], Chengguo Guan [a]

[a] State Key Laboratory of Palaeobiology and Stratigraphy, Nanjing Institute of Geology and Palaeontology, and Center for Excellence in Life and Palaeoenvironment, Chinese Academy of Sciences, Nanjing 210008, China
[b] University of Chinese Academy of Sciences, Beijing 100049, China
[c] State Key Laboratory of Biogeology and Environmental Geology, China University of Geosciences (Wuhan), Wuhan 430074, China
[d] Department of Geosciences, Virginia Tech, Blacksburg, VA 24061, USA

ARTICLE INFO

Keywords:
Ediacaran Period
Yangtze Block
Acanthomorphic acritarch
Carbon isotopic profile
Shuram excursion
Facies change

ABSTRACT

The Ediacaran Doushantuo Formation in South China documents profound biological and environmental changes after the Neoproterozoic global glaciations. However, since the geological records of these changes are scattered in various lithofacies, the establishment of the co-evolutionary pattern of life and environment largely relies on regional stratigraphic correlation. A negative $\delta^{13}C$ excursion in the upper Doushantuo Formation in the shelf-margin facies has been correlated with different $\delta^{13}C$ chemostratigraphic features in the Doushantuo Formation in the shelf-lagoon facies: either with EN3 (widely regarded as equivalent to the Shuram excursion in Oman) or with EN2, which occur respectively in the upper and middle Doushantuo Formation in the Yangtze Gorges area of South China. Here we report new litho-, chemo-, and biostratigraphic data of the Douoshantuo Formation at the Caojunba section in shelf-margin facies, where the lithostratigraphic sequence and carbon isotopic profile resemble those at other shelf-margin sections, e.g., the Yangjiaping and Zhongling sections. Diverse microfossils including nine genera and eighteen species of acanthomorphic acritarchs are found from the upper Doushantuo Formation at Caojunba, which represent to date the first report of the upper Doushantuo acritarch assemblage from the shelf-margin facies in South China. The newly recovered microfossil assemblage includes *Hocosphaeridium anozos*, *H. scaberfacium*, *Tanarium conoideum*, and clustered leiospheres, and these taxa support the stratigraphic correlation of upper Doushantuo Formation between shelf-margin and shelf-lagoon facies. This correlation indicates that the interval with negative $\delta^{13}C$ values in the upper Doushantuo Formation of shelf-margin facies is likely equivalent to EN3. This correlation also suggests that the $\delta^{13}C$ profiles of the EN3/Shuram excursion interval in different facies in South China have various expressions (e.g., stratigraphic range, magnitude), making its regional and continental correlations more challenging. On the other hand, the discovery of acritarch assemblage characteristic of the upper Doushantuo Formation in the Yangtze Gorges area from shelf-margin facies confirms their potential as an independent stratigraphic tool in the subdivision and correlation of Ediacaran strata.

1. Introduction

Following the Cryogenian global glaciations and preceding the Cambrian explosion, the Ediacaran Period (ca. 635–541 Ma) witnessed pivotal changes in the biosphere and Earth surface environment (Knoll et al., 2006; Narbonne et al., 2012; Xiao and Narbonne, 2020). The Ediacaran Doushantuo Formation in South China preserves various paleontological, sedimentological, and geochemical records of these changes (Zhou et al., 2019, and references therein), providing an unparalleled opportunity to uncover the co-evolution of Ediacaran life

* Corresponding author at: State Key Laboratory of Palaeobiology and Stratigraphy, Nanjing Institute of Geology and Palaeontology, and Center for Excellence in Life and Palaeoenvironment, Chinese Academy of Sciences, Nanjing 210008, China.
E-mail address: qouyang@nigpas.ac.cn (Q. Ouyang).

https://doi.org/10.1016/j.precamres.2022.106699
Received 24 January 2022; Received in revised form 27 April 2022; Accepted 30 April 2022
Available online 21 May 2022

and environment (e.g., Zhou et al., 2007; McFadden et al., 2008; Guan et al., 2014; Liu et al., 2014a; Wang et al., 2017b; Fan et al., 2021; Gan et al., 2021). However, the various geological records preserved in the Doushantuo Formation are distributed in different depositional facies (e.g., Xiao et al., 2014; Muscente et al., 2015), and their correlation is not straightforward due to facies changes (Jiang et al., 2011), hampering our understanding of the temporal and spatial relationships between these records.

Correlation of the Doushantuo Formation between the shelf-lagoon and shelf-margin facies of the Yangtze Platform in South China has long been open to debate (Kunimitsu et al., 2011; Cui et al., 2016; Furuyama et al., 2016). The uppermost Doushantuo Formation in shelf-margin areas hosts abundant calcite nodules with extremely negative $\delta^{13}C$ values (i.e., $< -30‰$), which were generally considered as geochemical evidence for anaerobic oxygenation of methane (AOM, e.g., Ader et al., 2009; Furuyama et al., 2016; Cui et al., 2017). The calcite nodule-bearing interval in shelf-margin facies has been correlated either with the Shuram excursion (or EN3 in South China) that represents the most profound negative carbon isotopic excursion in Earth history (e.g., Zhu et al., 2007; Ader et al., 2009; Jiang et al., 2011; Cui et al., 2016), or with an interval (e.g., the upper Member II of the Doushantuo Formation in the Yangtze Gorges area) that yields an earlier carbon isotopic excursion EN2 (Kunimitsu et al., 2011; Furuyama et al., 2016). The latter correlation was taken as evidence for a large sedimentary gap in the upper Doushantuo Formation, casting doubt on the stratigraphic completeness of the Doushantuo Formation in the shelf-margin environment (Furuyama et al., 2016). The former correlation, on the contrary, indicates that the magnitude and stratigraphic expression of EN3 are variable in different depositional facies, complicating its inter- and even intra-basinal correlations, but on the other hand, such variation provides new clues for the origin of the enigmatic Shuram excursion (Cui et al., 2021, 2022).

The above-mentioned correlation problem partially comes from the ambiguity of chemostratigraphic correlation based on stable isotopic excursions, which may not be unique to a specific stratigraphic interval. To resolve this problem, integrated stratigraphic data are needed. In this study, we report new litho-, chemo-, and biostratigraphic data from the shelf-margin Caojunba section in Hunan Province, South China. The newly recovered microfossils from the Caojunba section provide strong evidence for the correlation of the upper Doushantuo Formation between the shelf-lagoon and shelf-margin facies, with implications for the complexity of the carbon isotopic expression of the EN3/Shuram excursion interval. Furthermore, the diverse silicified microfossils, especially acanthomorphic acritarchs, from the Doushantuo Formation at Caojunba expand their paleogeographic distribution in South China, and help to test the stratigraphic application of the previously proposed biozonations established in the shelf-lagoon Yangtze Gorges area (McFadden et al., 2009; Liu et al., 2013; Xiao et al., 2014; Liu and Moczydłowska, 2019).

2. Geological settings

The Ediacaran strata on the Yangtze Block of South China were deposited on a passive continental margin (Wang and Li, 2003; Wang et al., 2021). In most areas of the Yangtze Block, the Ediacaran strata are composed of two formations: the Doushantuo Formation consisting of a mixture of siliciclastic and carbonate rocks, and the overlying Dengying Formation carbonate rocks in shallow-water settings or the Liuchapo/Piyuancun Formation banded chert in deep-water settings (Cao et al., 1989; Jiang et al., 2011). Across the shelf-to-basin transect in the Yangtze Block, lithostratigraphic sequence of the Doushantuo Formation shows significant facies changes (Fig. 1A, B; Jiang et al., 2011). Despite spatial changes in lithofacies, two depositional stages can be recognized in the Doushantuo Formation, including an early stage characterized by siliciclastic deposits, and a later stage characterized by dominant carbonate precipitations in shallower water environments

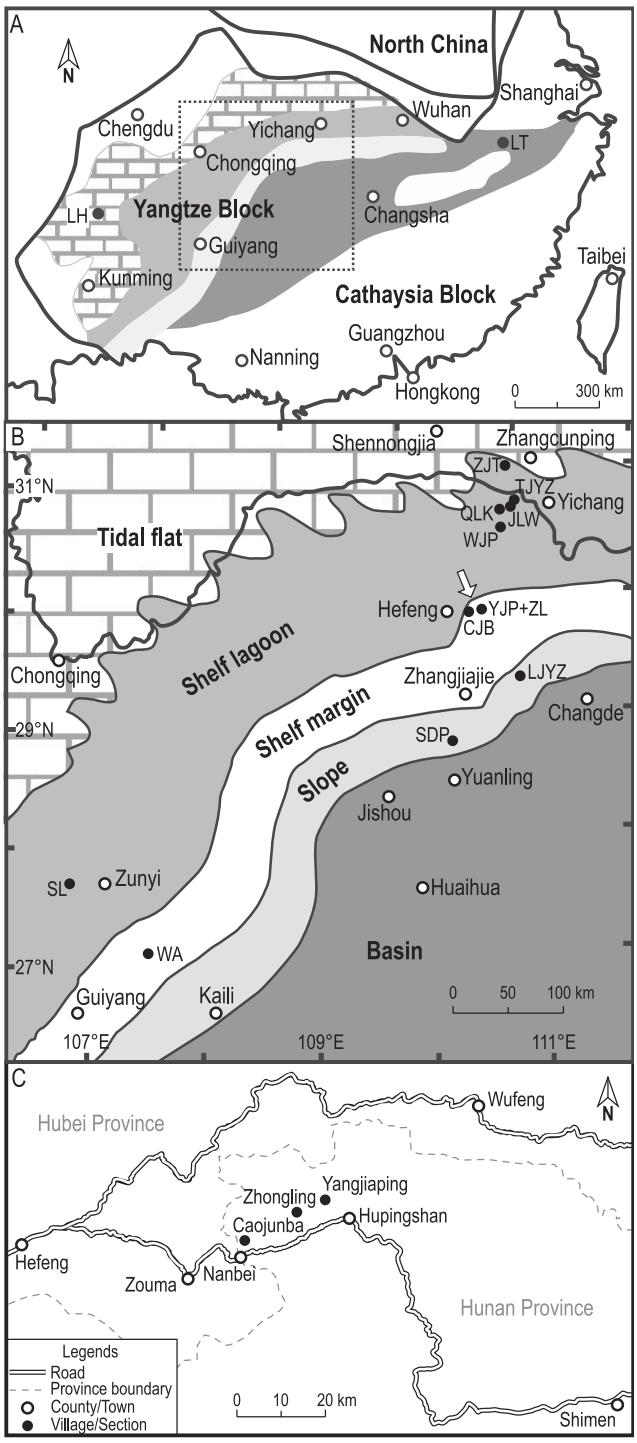

Fig. 1. Paleogeographic and transportation maps showing location of study sections. (A) Paleogeographic map of the Yangtze Block in the Ediacaran Period. (B) Magnification of area marked by rectangle in (A). (C) Detailed map (arrow in B) showing location of the Caojunba, Yangjiaping, and Zhongling sections. (A) and (B) are modified from Jiang et al. (2011). Abbreviations in (A) and (B) denote stratigraphic sections (areas) discussed in this study: LH, Lianghong section (Wang et al., 2012); QLK, Qinglinkou section, ZJT, Zhengjiatang section, JLW, Jiulongwan section, and TJYZ, Tianjiayuanzi section (Zhou et al., 2017); WJP, Wangjiapeng section (Lan et al., 2019); SL, Songlin area (Shang et al., 2019); CJB, Caojunba section (this study); YJP, Yangjiaping section (Ader et al., 2009; this study); ZL, Zhongling section (Cui et al., 2017); WA, Weng'an area (Xiao et al., 2014); LJYZ, Lujiayuanzi section (Ouyang et al., 2017); SDP, Siduping section (Wang et al., 2016); LT, Lantian section (Yuan et al., 2011).

(Vernhet and Reijmer, 2010; Jiang et al., 2011).

The Caojunba section (GPS: 29°53′53″ N, 110°32′54″ E) near the Caojunba village, Shimen County, Hunan Province, was located in the shelf-margin facies in the Ediacaran Period (Fig. 1B, C). In this area, Neoproterozoic strata consist of, in ascending order, the Tonian Banxi Group, the Cryogenian Xieshuihe, Dongshanfeng, Datangpo, and Nantuo formations, and the Ediacaran Doushantuo and Dengying formations (Zhou et al., 2004). The exposed strata of the Doushantuo Formation at the Caojunba section can be subdivided into a lower calcareous shale interval (ca. 70 m, not including the cap dolostone and lower parts of shales that were covered by vegetation; Figs. 2, 3A, B, 4A) and an upper carbonate interval (ca. 66 m available, Figs. 2, 3A). Millimeter- to centimeter-sized, partially calcified cherty nodules occur commonly in the shale interval (Fig. 3C). The lowermost 20 m of the carbonate interval is thin- to thick-bedded, partially silicified dolostone containing cherty bands and rare cherty nodules. This interval is overlain by ca. 5 m of medium-bedded dolostone with thin dolomitic shale layers (Fig. 3D). Further upsection, there is ca. 10 m of thick-bedded and occasionally laminated dolostone intercalated with cherty bands (Fig. 3E) and purplish shale, and silicified intraclastic beds (Fig. 4B) and breccias occasionally occur in its upper part, possibly representing storm deposits (Fig. 3F). Still upsection is ca. 31 m of thin-bedded dolostone with two lenticular grainstone beds composed mostly of millimeter-sized, silicified pisoids, indicating an intertidal to shallow subtidal environment (Fig. 3G). White, irregular-shaped calcite nodules composed of coarse calcite crystals and a quartz rim (Fig. 3H, 4C–E) occur in the upper 46 m of the carbonate interval, and are most abundant in strata about 45 to 55 m above the base of the carbonate interval, in which the calcite nodules commonly occur in layers (Fig. 3I). Several dolostone beds containing black centimeter-sized cherty nodules (Fig. 3J) also occur in the calcite nodule-rich interval. Noteworthy is that the uppermost 11 m strata yield fewer calcite nodules compared with the underlying strata, but contain unevenly distributed calcite cements (Fig. 4F). Phosphorite beds as a regional lithostratigraphic marker for the boundary between the Doushantuo and Dengying formations were not observed at the Caojunba section, and the carbonate interval is tentatively considered to represent the upper Doushantuo Formation, with its upper boundary undefined due to poor exposure.

The Doushantuo Formation in shelf-margin facies is best represented at the Yangjiaping section, ca. 20 km to the northeast of the Caojunba section (Fig. 1B). At Yangjiaping, the Doushantuo Formation above the cap dolostone also comprises a lower argillaceous interval and an upper carbonate interval, with abundant intraclasts and calcite nodules in the upper part of the carbonate interval (Fig. 5). The Yangjiaping section has been thoroughly investigated by many previous researchers, and detailed lithostratigraphic sequence can be found in Cui et al. (2016) and references therein.

The Doushantuo Formation in the Yangtze Gorges area where the stratotype section is located was deposited in a shelf-lagoon environment and has long been used as the yardstick for the regional correlation

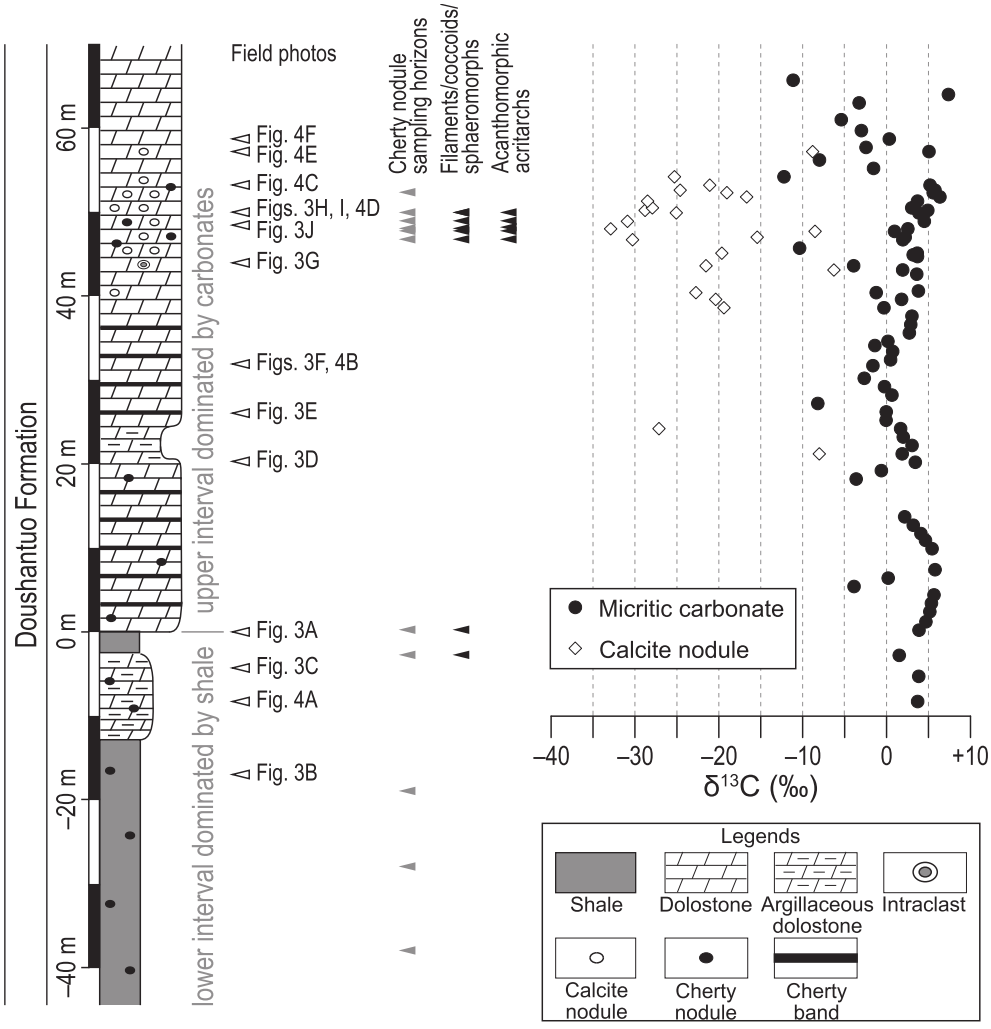

Fig. 2. Lithostratigraphic sequence, carbon isotopic profile, cherty nodule sampling horizons, and microfossil occurrences of the Doushantuo Formation at the Caojunba section. Stratigraphic horizons of the field photographs in Fig. 3 are marked in the log.

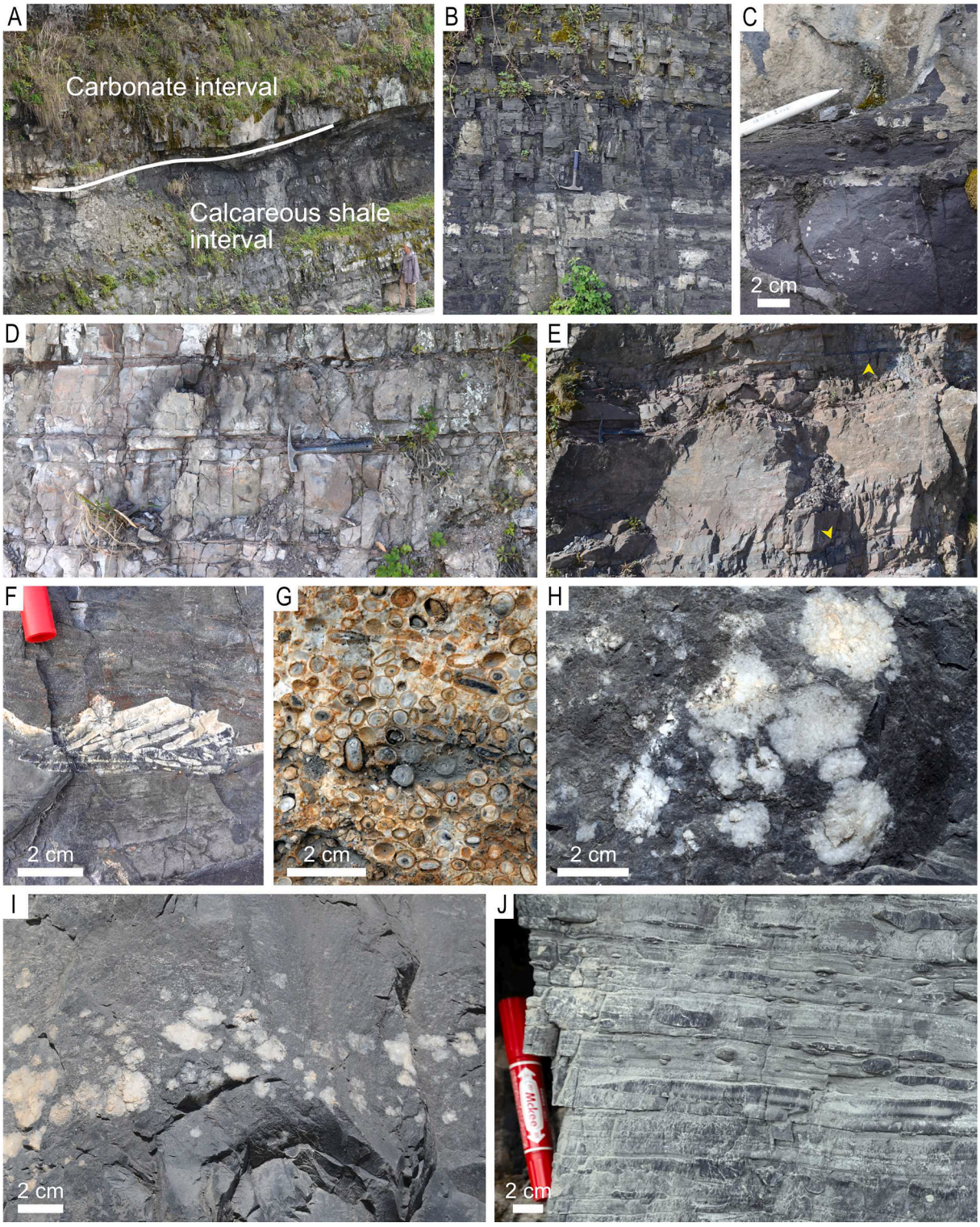

Fig. 3. Field photographs of the Doushantuo Formation at the Caojuba section. Stratigraphic horizons of each image are marked in Fig. 2. (A) Boundary between the lower calcareous shale interval and the upper carbonate interval. (B) Calcareous shale and argillaceous dolostone in the lower part of the section. (C) Millimeter-sized cherty nodules in the calcareous shale interval. (D) Dolostone with shale intercalations. (E) Dolostone intercalated with cherty bands (denoted by yellow arrowheads). (F) Reworked breccia on an erosional surface from thin- to medium-bedded dolostone in the middle part of the carbonate interval. (G) Silicified pisoids from medium- to thick-bedded dolostone in the upper part of the carbonate interval. (H) Calcite nodules from the upper part of the carbonate interval. (I) Calcite nodule-rich dolostone bed in the upper part of the carbonate interval. (J) Centimeter-sized cherty nodules in the upper part of the carbonate interval. Hammers in (B), (D), and (E) are ca. 27 cm long.

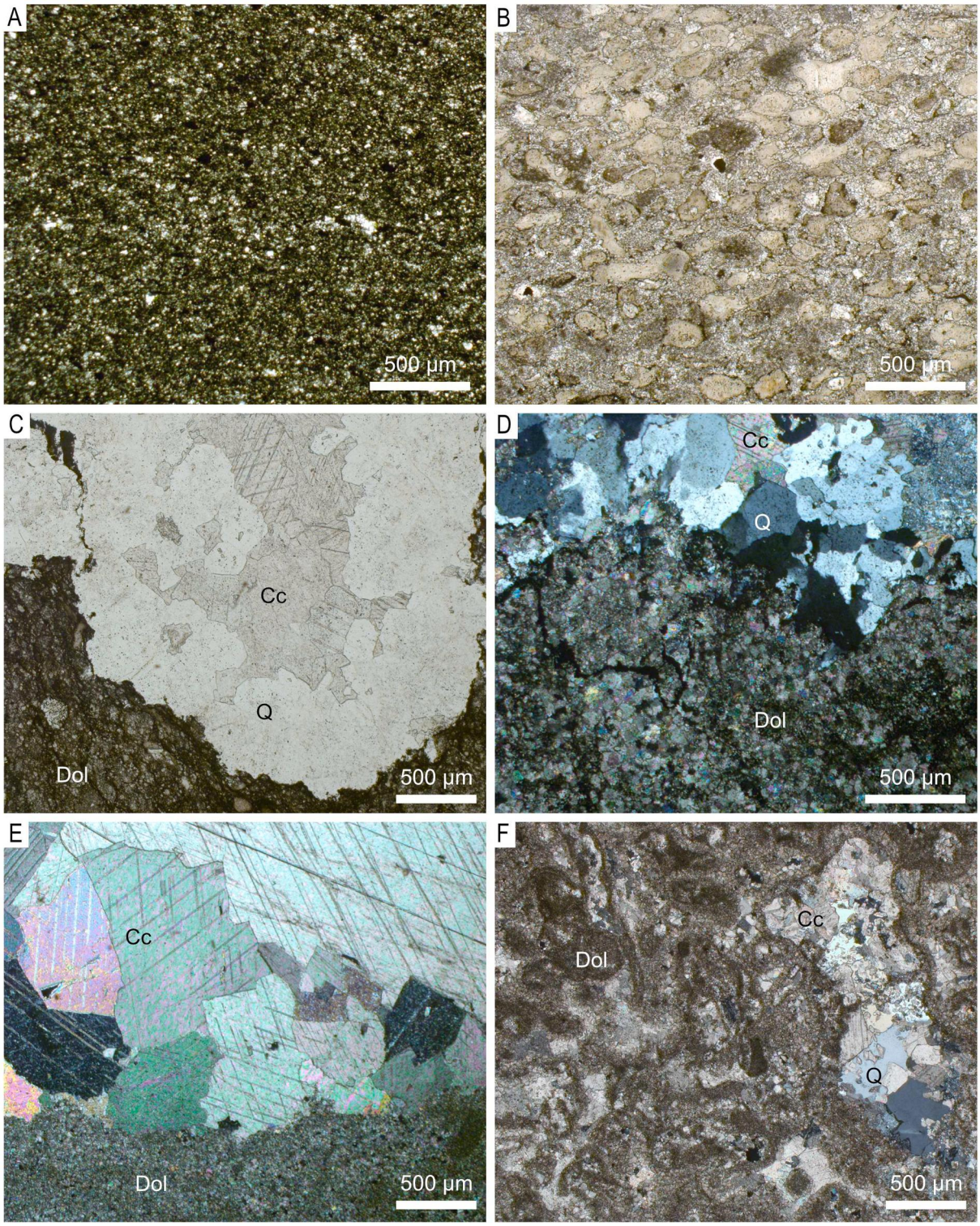

Fig. 4. Thin-section petrographic photomicrographs of the Doushantuo Formation at the Caojuba section under cross-polarized light (XPL) and plane-polarized light (PPL). Stratigraphic horizons of each image are marked in Fig. 2. (A) Argillaceous dolostone in the lower part of the section, PPL. (B) Partially silicified dolostone with abundant intraclasts in the lower part of the carbonate interval, PPL. (C) Calcite nodule with a quartz rim and the micritic dolostone matrix, PPL. (D) Quartz rim of a calcite nodule and surrounding dolomicrites, XPL. (E) Calcite nodule and the micritic dolostone matrix, XPL. (F) Micritic clotted structures and peloids with recrystallized calcite cements in the upper part of the carbonate interval, XPL. Abbreviations: Cc, calcite; Qz, quartz; Dol, dolomite.

of the Doushantuo Formation because of the availability of integrated stratigraphic and paleontological records (McFadden et al., 2008; Jiang et al., 2011; Zhou et al., 2019). Lithostratigraphically, the Doushantuo Formation in the Yangtze Gorges area has been subdivided into four members (represented by the Jiulongwan section in Fig. 5): Member I (cap dolostone), Member II (argillaceous dolostone or calcareous shale, representing the early depositional stage), Member III (dominated by carbonate rocks, representing majority of the later stage of Doushantuo deposition), and Member IV (black shale) (Wang et al., 1998; Zhou and Xiao, 2007). Three negative $\delta^{13}C$ excursions have been recognized in

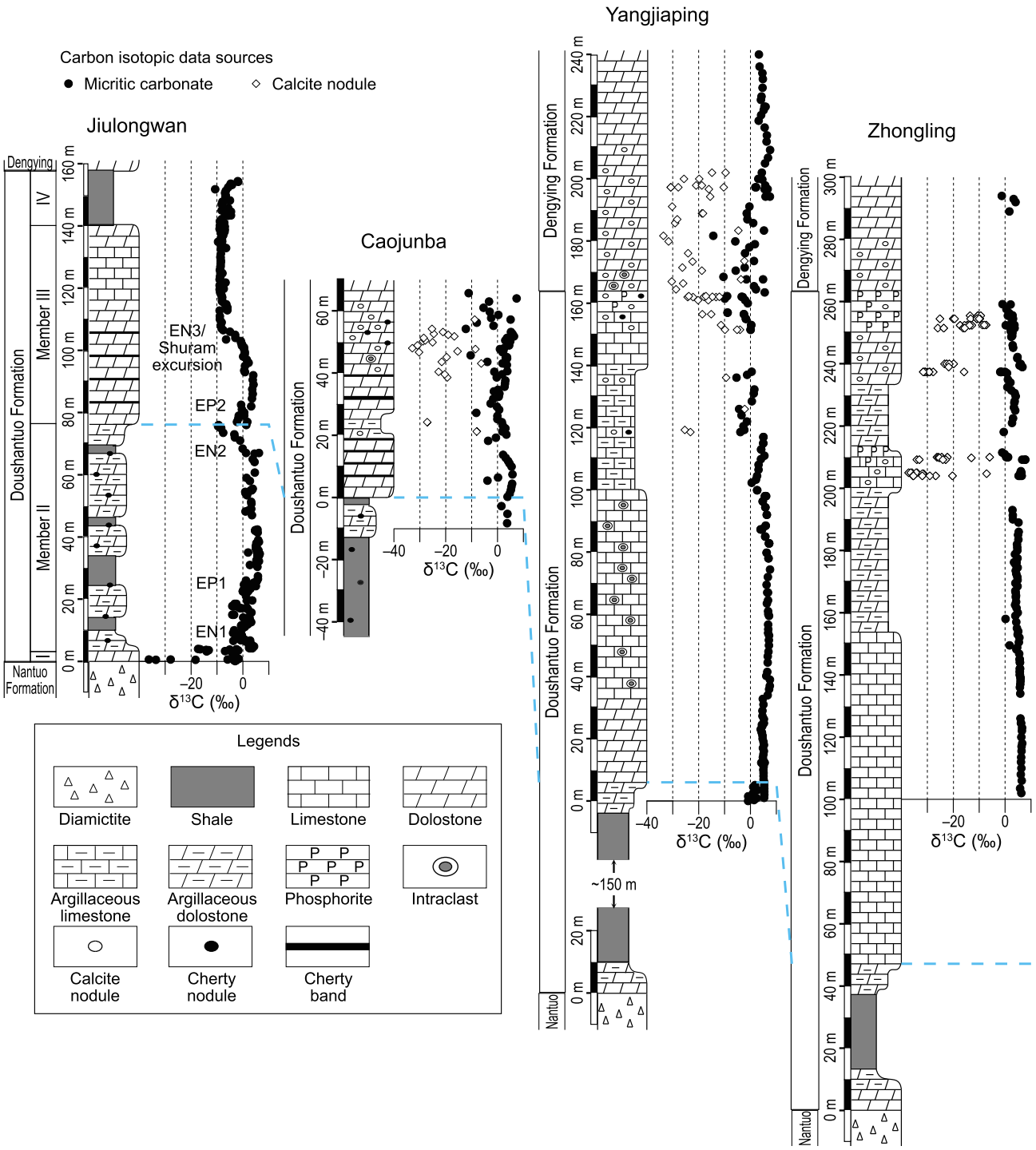

Fig. 5. Lithostratigraphic sequences and carbon isotopic profiles of the Doushantuo Formation at the shelf-lagoon Jiulongwan section and the shelf-margin Caojunba, Yangjiaping, and Zhongling sections. Carbon isotopic data for the Jiulongwan and Zhongling sections are from McFadden et al. (2008) and Cui et al. (2017), respectively, with data for cap dolostone at the Zhongling sections omitted. Blue dash lines denote presumed correlations.

Member I (EN1), upper Member II (EN2) and middle–upper Member III (EN3). These negative excursions are separated by two positive $\delta^{13}C$ excursions: EP1 between EN1 and EN2, and EP2 between EN2 and EN3 (Fig. 5; Jiang et al., 2007; Zhou and Xiao, 2007). These excursions have been accepted as roughly synchronous and widely applied to the correlation of the Doushantuo Formation across different facies in the Yangtze block (e.g., Jiang et al., 2011; Li et al., 2016; Wang et al., 2016; Wang et al., 2017a; Ouyang et al., 2019). Within this framework, it is worth pointing out that the lithostratigraphic sequence and chemostratigraphic profile of Member III are highly variable in the Yangtze Gorges area (An et al., 2015; Zhou et al., 2017), likely indicating a shallow water environment that is sensitive to facies variations related to local sea-level changes.

3. Materials and methods

Seventy-two carbonate samples were collected at the Caojunba section for stable isotopic analyses, with three samples from the uppermost 10 m of the calcareous shale interval and 69 samples from the carbonate interval (Table 1). Stratigraphic heights were measured from a datum

Table 1
Carbon and oxygen isotopic data and cherty nodule sampling horizons at the Caojunba section.

Sample	Stratigraphic height(m)	$\delta^{13}C_{carb}$ (‰)	$\delta^{18}O_{carb}$ (‰)	Lithology	Formation
21CJB-1–2	65.7	–11.1	–7.5	Dolostone	Doushantuo
21CJB-2–2	64	+7.4	–4.9	Dolostone	Doushantuo
21CJB-3–2	63	–3.3	–6.5	Dolostone	Doushantuo
21CJB-4–2	61	–5.4	–7.5	Dolostone	Doushantuo
21CJB-5–2	59.7	–3.0	–6.4	Dolostone	Doushantuo
21CJB-6–2	58.7	+0.3	–5.8	Dolostone	Doushantuo
21CJB-7–2	57.7	–2.4	–6.2	Dolostone	Doushantuo
21CJB-8–2	57.2	+5.1	–4.3	Dolostone	Doushantuo
21CJB-8–1	57.2	–8.8	–10.8	Calcite nodule	Doushantuo
21CJB-9–2	56.2	–8.0	–7.3	Dolostone	Doushantuo
21CJB-10–2	55.2	–1.6	–5.8	Dolostone	Doushantuo
21CJB-11–2	54.2	–12.2	–7.7	Dolostone	Doushantuo
21CJB-11–1	54.2	–25.3	–8.0	Calcite nodule	Doushantuo
21CJB-12–2	53.2	+5.2	–3.8	Dolostone	Doushantuo
21CJB-12–1	53.2	–21.1	–8.4	Calcite nodule	Doushantuo
21CJB-13–2	52.6	+5.8	–3.4	Dolostone	Doushantuo
21CJB-13–1	52.6	–24.6	–8.6	Calcite nodule	Doushantuo
21DC-1	52.3			Cherty nodule	Doushantuo
21CJB-14–2	52.3	+5.6	–3.8	Dolostone	Doushantuo
21CJB-14–1	52.3	–19.0	–10.1	Calcite nodule	Doushantuo
21CJB-15–2	51.8	+6.4	–3.7	Dolostone	Doushantuo
21CJB-15–1	51.8	–16.7	–8.5	Calcite nodule	Doushantuo
21CJB-16–2	51.3	+3.7	–4.5	Dolostone	Doushantuo
21CJB-16–1	51.3	–28.5	–10.5	Calcite nodule	Doushantuo
21CJB-17–2	50.5	+3.0	–4.4	Dolostone	Doushantuo
21CJB-17–1	50.5	–27.9	–10.2	Calcite nodule	Doushantuo
21CJB-18–2	50.2	+4.9	–4.1	Dolostone	Doushantuo
21CJB-18–1	50.2	–28.8	–9.9	Calcite nodule	Doushantuo
21DC-2	49.9			Cherty nodule	Doushantuo
21CJB-19–2	49.9	+3.8	–4.0	Dolostone	Doushantuo
21CJB-19–1	49.9	–25.1	–9.0	Calcite nodule	Doushantuo
21DC-3	48.9			Cherty nodule	Doushantuo
21CJB-20–2	48.9	+4.5	–3.2	Dolostone	Doushantuo
21CJB-20–1	48.9	–30.9	–8.7	Calcite nodule	Doushantuo
21DC-6	48			Cherty nodule	Doushantuo
21CJB-21–2	48	+2.5	–4.2	Dolostone	Doushantuo
21CJB-21–1	48	–32.9	–9.6	Calcite nodule	Doushantuo
21DC-4	47.7			Cherty nodule	Doushantuo
21CJB-22–1	47.7	–8.5	–8.5	Calcite nodule	Doushantuo
21CJB-22–2	47.7	+1.0	–4.4	Argillaceous dolostone	Doushantuo
21CJB-23–1	47	–15.4	–10.2	Calcite nodule	Doushantuo
21CJB-23–2	47	+2.2	–3.8	Argillaceous dolostone	Doushantuo
21DC-5	46.7			Cherty nodule	Doushantuo
21CJB-24–2	46.7	+1.9	–3.9	Dolostone	Doushantuo
21CJB-24–1	46.7	–30.3	–9.3	Calcite nodule	Doushantuo
21CJB-25–2	45.7	–10.4	–7.8	Dolostone	Doushantuo
21CJB-26–2	45.1	+3.7	–4.8	Dolostone	Doushantuo
21CJB-26–1	45.1	–19.6	–9.0	Calcite nodule	Doushantuo
21CJB-27–2	44.9	+3.2	–4.9	Dolostone	Doushantuo
21CJB-28–2	44.7	+3.7	–5.4	Dolostone	Doushantuo
21CJB-30–2	43.6	–3.9	–7.0	Dolostone	Doushantuo
21CJB-30–1	43.6	–21.5	–11.2	Calcite nodule	Doushantuo
21CJB-31–2	43.1	+1.9	–4.7	Dolostone	Doushantuo
21CJB-31–1	43.1	–6.3	–9.2	Calcite nodule	Doushantuo
21CJB-32–2	42.6	+3.6	–5.3	Dolostone	Doushantuo
21CJB-34–2	40.6	+3.8	–5.5	Dolostone	Doushantuo
21CJB-35–2	40.4	–1.2	–6.2	Dolostone	Doushantuo
21CJB-35–1	40.4	–22.7	–9.7	Calcite nodule	Doushantuo
21CJB-36–2	39.6	+1.8	–5.5	Dolostone	Doushantuo
21CJB-36–1	39.6	–20.4	–9.8	Calcite nodule	Doushantuo
21CJB-37–2	38.6	–0.3	–6.4	Dolostone	Doushantuo
21CJB-37–1	38.6	–19.4	–9.9	Calcite nodule	Doushantuo
21CJB-38–2	37.6	+3.0	–5.4	Dolostone	Doushantuo
21CJB-39–2	36.6	+2.9	–5.6	Dolostone	Doushantuo
21CJB-40–2	35.6	+2.7	–5.8	Dolostone	Doushantuo
21CJB-41–2	34.6	+0.2	–4.5	Dolostone	Doushantuo
21CJB-43–2	34.1	–1.4	–2.6	Dolostone	Doushantuo
21CJB-42–2	33.4	+0.7	–2.8	Dolostone	Doushantuo
21CJB-44–2	32.4	+0.5	–3.2	Dolostone	Doushantuo
21CJB-45–2	31.7	–1.6	–4.5	Dolostone	Doushantuo
21CJB-46–2	30.2	–2.7	–5.6	Dolostone	Doushantuo
21CJB-47–2	29.2	–0.2	–2.7	Dolostone	Doushantuo
21CJB-48–2	28.2	+0.6	–3.2	Dolostone	Doushantuo

(*continued on next page*)

Table 1 (*continued*)

Sample	Stratigraphic height(m)	$\delta^{13}C_{carb}$ (‰)	$\delta^{18}O_{carb}$ (‰)	Lithology	Formation
21CJB-49–2	27.2	–8.2	–9.9	Dolostone	Doushantuo
21CJB-50–2	26.2	–0.0	–6.2	Dolostone	Doushantuo
21CJB-51–2	25.2	–0.1	–5.2	Dolostone	Doushantuo
21CJB-52–1	24.2	–27.1	–9.8	Calcite nodule	Doushantuo
21CJB-52–2	24.2	+1.7	–5.4	Argillaceous dolostone	Doushantuo
21CJB-53–2	23.2	+2.0	–6.1	Argillaceous dolostone	Doushantuo
21CJB-54–2	22.2	+3.0	–5.1	Argillaceous dolostone	Doushantuo
21CJB-55–1	21.2	–8.0	–7.8	Calcite nodule	Doushantuo
21CJB-55–2	21.2	+1.9	–4.1	Argillaceous dolostone	Doushantuo
21CJB-56–2	20.2	+3.4	–2.4	Dolostone	Doushantuo
21CJB-57–2	19.2	–0.6	–4.4	Dolostone	Doushantuo
21CJB-58–2	18.2	–3.6	–7.4	Dolostone	Doushantuo
21CJB-59–2	13.7	+2.2	–5.8	Dolostone	Doushantuo
21CJB-60–2	12.7	+3.2	–5.3	Dolostone	Doushantuo
21CJB-61–2	11.7	+4.1	–5.1	Dolostone	Doushantuo
21CJB-62–2	10.9	+4.6	–5.7	Dolostone	Doushantuo
21CJB-63–2	9.9	+5.4	–5.1	Dolostone	Doushantuo
21CJB-64–2	7.4	+5.8	–4.9	Dolostone	Doushantuo
21CJB-65–2	6.4	+0.2	–6.6	Dolostone	Doushantuo
21CJB-66–2	5.4	–3.9	–6.3	Dolostone	Doushantuo
21CJB-67–2	4.4	+5.7	–3.7	Dolostone	Doushantuo
21CJB-68–2	3.4	+5.3	–4.0	Dolostone	Doushantuo
21CJB-69–2	2.4	+5.2	–3.7	Dolostone	Doushantuo
21CJB-70–2	1.2	+4.7	–4.7	Dolostone	Doushantuo
21CJB-71–2	0.2	+3.9	–4.9	Dolostone	Doushantuo
21CJB-72	0.2			Cherty nodule	Doushantuo
21CJB-74–2	–2.8	+1.5	–3.2	Calcareous shale	Doushantuo
21CJB-74	–2.8			Cherty nodule	Doushantuo
21CJB-75–2	–5.3	+3.8	–3.2	Dolostone	Doushantuo
21CJB-76–2	–8.3	+3.7	–2.3	Calcareous shale	Doushantuo
21CJB-79	–19			Cherty nodule	Doushantuo
21CJB-81	–28			Cherty nodule	Doushantuo
21CJB-82	–38			Cherty nodule	Doushantuo

* Stratigraphic height is measured from an arbitrary datum (0 m) at the boundary between the calcareous shale interval and the carbonate interval. In some samples, calcite nodules and the carbonate matrix were micro-drilled and analyzed separately. The 24 measurements of calcite nodules are labeled with the suffix −1, and measurements of the matrix are labeled with the suffix −2.

that separates the lower shaly interval and the upper carbonate interval. Thin sections for petrographic observation were made for selected samples. Powders of all samples were micro-drilled from polished slabs for $\delta^{13}C$ and $\delta^{18}O$ analyses. For 24 carbonate rock samples containing calcite nodules, the micritic matrices and nodules were micro-drilled and analyzed separately.

One hundred and fifty-four calcareous mudstone and carbonate samples were collected from the middle–upper Doushantuo Formation and lower Dengying Formation (ca. 240 m thick) at the Yangjiaping section for $\delta^{13}C$ and $\delta^{18}O$ analyses (Table 2). Stratigraphic heights were measured from an arbitrary datum near the base of the upper Doushantuo carbonate interval. Petrographic observations were conducted before micro-drilling on each sample. Forty-four samples contain calcite nodules, among which 41 were micro-drilled on both calcite nodules and corresponding micritic matrix, and three only on calcite nodules. Some samples were micro-drilled at different locations on the same slab for replicate analyses. Analytical results are plotted in Fig. 5 and presented in Table 2, with the sample numbers followed by suffixes denoting replicate analyses whenever applicable.

Isotopic analysis was conducted in the State Key Laboratory of Palaeobiology and Stratigraphy, Nanjing Institute of Geology and Palaeontology, Chinese Academy of Sciences. An aliquot of 80–100 μg powder of each sample was allowed to react with orthophosphoric acid for 150–200 s at 72 ℃ in a Kiel IV carbonate device coupled with a MAT 253 isotope ratio mass spectrometer. The working standard GBW-04405 was used to monitor the EA-IRMS system. CO_2 gas calibrated against the NBS19 standard was used as reference gas. The analytical precision (1σ) was better than ± 0.04‰ for $\delta^{13}C$ and ± 0.08‰ for $\delta^{18}O$. Results are expressed in the conventional δ-notation versus the VPDB standard.

Eleven cherty nodule samples from the Caojunba section were collected for micropaleontological study, including six (with the prefix 21DC-) from the ca. 10 m-thick calcite nodule-rich interval in the upper part of the section, and five (with the prefix 21CJB-) from the upper 40 m of the argillaceous interval below the zero datum and the basal 1-m-thick carbonate interval above the zero datum (Fig. 2, Appendix 1). One hundred and four thin sections (all cut parallel to bedding surfaces) from the Caojunba section were made for the cherty nodule samples, including 78 for samples with the prefix 21DC- and 26 for samples with the prefix 21CJB-. These thin sections were examined under plain- and cross-polarized light using a ZEISS Scope A1 microscope. Microfossils were recorded with stage coordinates and photographed by an Olympic DP74 digital camera attached to the microscope. All thin sections and specimens are reposited in the Nanjing Institute of Geology and Palaeontology, Chinese Academy of Sciences.

4. Results

4.1. Carbon and oxygen isotopic compositions

Carbon and oxygen isotopic composition data of the Doushantuo Formation at the Caojunba section are presented in Table 1, with $\delta^{13}C$ data plotted in Fig. 2. Excluding the calcite nodule samples, the $\delta^{13}C$ values from the Caojunba section range from − 12.2‰ to + 7.4‰ for the entire sampled strata, and the $\delta^{18}O$ values vary between − 9.9‰ and − 2.3‰. The uppermost 10 m of the calcareous shale interval and the lower ca. 50 m of the carbonate interval are characterized by variable but positive $\delta^{13}C$ values up to + 6‰, with several $\delta^{13}C$ values around 0‰ occurring at ca. 30 m above the base of the carbonate interval. The uppermost ca. 15 m of dolostones containing rare calcite nodule beds and some calcite cements record scattered $\delta^{13}C$ values that range from − 12.2‰ to + 7.4‰. $\delta^{13}C$ values of the calcite nodules are significantly lower than those of carbonate matrix, ranging from − 32.9‰ to − 6.3‰,

Table 2
Carbon and oxygen isotopic data of the studied samples at the Yangjiaping section.

Sample	Stratigraphic height(m)	$\delta^{13}C_{carb}$ (‰)	$\delta^{18}O_{carb}$ (‰)	Lithology	Formation
16YJP-170	0	–0.9	–5.7	Argillaceous dolomite	Doushantuo
16YJP-171	0.3	+1.3	–2.0	Argillaceous dolomite	Doushantuo
16YJP-172	0.9	+2.4	–3.5	Argillaceous dolomite	Doushantuo
16YJP-1	1	+5.3	–3.3	Dolomite	Doushantuo
16YJP-173	1.5	–0.9	–7.8	Argillaceous dolomite	Doushantuo
16YJP-2	2	+5.3	–4.2	Dolomite	Doushantuo
16YJP-174	2.5	+1.0	–7.5	Argillaceous dolomite	Doushantuo
16YJP-3	3	+5.3	–4.8	Dolomite	Doushantuo
16YJP-175	3.5	+2.7	–2.9	Argillaceous dolomite	Doushantuo
16YJP-4	4	+5.3	–5.1	Dolomite	Doushantuo
16YJP-176	4.5	+1.1	–4.9	Argillaceous dolomite	Doushantuo
16YJP-5	5	+5.3	–4.9	Dolomite	Doushantuo
16YJP-177	5.1	+1.8	–6.4	Argillaceous dolomite	Doushantuo
16YJP-6	6	+5.3	–5.5	Dolomite	Doushantuo
16YJP-7	6.9	+5.0	–5.9	Dolomite	Doushantuo
16YJP-8	8	+5.0	–6.5	Dolomite	Doushantuo
16YJP-9	9	+5.0	–7.0	Dolomite	Doushantuo
16YJP-10	10	+5.0	–6.5	Dolomite	Doushantuo
16YJP-11	11	+5.1	–6.9	Dolomite	Doushantuo
16YJP-12	12	+4.6	–5.7	Dolomite	Doushantuo
16YJP-13–1	12.3	+4.2	–6.9	Dolomite	Doushantuo
16YJP-13–2	12.3	+5.5	–8.2	Dolomite	Doushantuo
16YJP-14	13	+5.0	–5.4	Dolomite	Doushantuo
16YJP-15	14	+4.8	–4.8	Dolomite	Doushantuo
16YJP-16	15	+5.0	–4.8	Dolomite	Doushantuo
16YJP-17	16	+5.2	–4.1	Dolomite	Doushantuo
16YJP-18	17	+4.8	–5.3	Dolomite	Doushantuo
16YJP-19	18	+5.2	–6.2	Dolomite	Doushantuo
16YJP-20	19	+5.0	–5.7	Dolomite	Doushantuo
16YJP-21	20	+4.7	–6.0	Dolomite	Doushantuo
16YJP-22	21	+4.7	–6.0	Dolomite	Doushantuo
16YJP-23–1	22	+4.4	–6.2	Dolomite	Doushantuo
16YJP-23–2	22	+4.4	–6.4	Dolomite	Doushantuo
16YJP-24	23	+3.9	–7.1	Dolomite	Doushantuo
16YJP-25–1	24	+4.5	–6.4	Dolomite	Doushantuo
16YJP-26–2	24.5	+4.4	–5.0	Dolomite	Doushantuo
16YJP-27	25	+5.2	–5.5	Dolomite	Doushantuo
16YJP-28	26.3	+5.2	–5.7	Dolomite	Doushantuo
16YJP-29	27.3	+4.6	–5.7	Dolomite	Doushantuo
16YJP-30	29	+4.6	–6.3	Dolomite	Doushantuo
16YJP-31	31	+5.0	–5.6	Dolomite	Doushantuo
16YJP-32	32.8	+4.8	–5.5	Dolomite	Doushantuo
16YJP-33	34	+6.6	–7.9	Dolomite	Doushantuo
16YJP-34	35.9	+7.2	–7.7	Limestone	Doushantuo
16YJP-35	37	+7.5	–7.8	Limestone	Doushantuo
16YJP-36	39	+7.5	–7.4	Limestone	Doushantuo
16YJP-37	40.2	+6.1	–7.2	Limestone	Doushantuo
16YJP-38	41.5	+6.5	–7.0	Limestone	Doushantuo
16YJP-39	44.5	+6.6	–6.6	Limestone	Doushantuo
16YJP-40	46.5	+6.7	–7.1	Limestone	Doushantuo
16YJP-41	48	+6.9	–7.1	Limestone	Doushantuo
16YJP-42	50	+7.1	–6.8	Limestone	Doushantuo
16YJP-43	51.7	+7.1	–7.0	Limestone	Doushantuo
16YJP-44	53.2	+7.2	–6.7	Limestone	Doushantuo
16YJP-45	54	+6.8	–6.8	Limestone	Doushantuo
16YJP-46	55.2	+6.9	–6.9	Limestone	Doushantuo
16YJP-47	56.7	+6.8	–7.0	Limestone	Doushantuo
16YJP-48	59.5	+7.2	–5.0	Limestone	Doushantuo
16YJP-49	60.1	+6.9	–6.1	Limestone	Doushantuo
16YJP-50	61	+6.8	–6.6	Limestone	Doushantuo
16YJP-51	63.5	+6.3	–6.8	Limestone	Doushantuo
16YJP-52	64.5	+6.8	–7.1	Limestone	Doushantuo
16YJP-54–1	67	+6.8	–6.8	Limestone	Doushantuo
16YJP-54–2	67	+6.5	–6.5	Limestone	Doushantuo
16YJP-55	69.5	+6.2	–6.8	Limestone	Doushantuo
16YJP-56	72	+6.7	–6.5	Limestone	Doushantuo
16YJP-57	74.4	+7.6	–6.6	Limestone	Doushantuo
16YJP-58	78	+7.0	–6.5	Limestone	Doushantuo
16YJP-59	79.8	+6.2	–6.9	Limestone	Doushantuo
16YJP-60–1	82.8	+7.1	–7.3	Limestone	Doushantuo
16YJP-60–2	82.8	+7.2	–7.1	Limestone	Doushantuo
16YJP-61	85	+5.7	–7.5	Limestone	Doushantuo
16YJP-62–1	87.3	+3.9	–5.8	Limestone	Doushantuo

(*continued on next page*)

Table 2 (*continued*)

Sample	Stratigraphic height(m)	$\delta^{13}C_{carb}$ (‰)	$\delta^{18}O_{carb}$ (‰)	Lithology	Formation
16YJP-62–2	87.3	+4.5	–7.5	Limestone	Doushantuo
16YJP-63	88.5	+5.9	–7.8	Limestone	Doushantuo
16YJP-64	92	+6.3	–7.1	Limestone	Doushantuo
16YJP-65	94.4	+5.8	–7.3	Limestone	Doushantuo
16YJP-66	96.3	+4.7	–4.5	Limestone	Doushantuo
16YJP-67–1	98	+6.0	–5.7	Limestone	Doushantuo
16YJP-67–2	98	+5.6	–6.5	Limestone	Doushantuo
16YJP-68	99.9	+2.6	–6.0	Limestone	Doushantuo
16YJP-70	102.3	+0.5	–4.3	Calcareous mudstone	Doushantuo
16YJP-71	103.3	+2.1	–1.9	Calcareous mudstone	Doushantuo
16YJP-72	104.5	+2.6	–2.7	Calcareous mudstone	Doushantuo
16YJP-73	106.5	+3.1	–3.8	Calcareous mudstone	Doushantuo
16YJP-74	108.1	+3.1	–1.5	Calcareous mudstone	Doushantuo
16YJP-75	109.9	+4.0	–4.2	Calcareous mudstone	Doushantuo
16YJP-76	111	+5.4	–6.6	Calcareous mudstone	Doushantuo
16YJP-77	113	+4.1	–8.1	Micrite	Doushantuo
16YJP-78	115	+4.9	–6.9	Micrite	Doushantuo
16YJP-79	117	+5.0	–3.6	Micrite	Doushantuo
16YJP-80–1	118.6	–23.2	–9.3	Calcite nodule	Doushantuo
16YJP-80–2	118.6	–3.9	–5.2	Argillaceous limestone	Doushantuo
16YJP-81–1	119.3	–25.4	–8.8	Calcite nodule	Doushantuo
16YJP-81–2	119.3	–2.4	–5.5	Argillaceous limestone	Doushantuo
16YJP-82	120.5	–2.7	–3.7	Argillaceous limestone	Doushantuo
16YJP-83	122	–1.4	–3.9	Argillaceous limestone	Doushantuo
16YJP-84	124	–3.5	–2.4	Argillaceous limestone	Doushantuo
16YJP-85–1	126	–2.2	–7.2	Calcite nodule	Doushantuo
16YJP-85–2	126	–4.4	–5.1	Argillaceous limestone	Doushantuo
16YJP-86	128.5	+0.5	–3.1	Argillaceous limestone	Doushantuo
16YJP-87	131	+1.3	–3.6	Argillaceous limestone	Doushantuo
16YJP-88	132.3	+1.5	–2.9	Argillaceous limestone	Doushantuo
16YJP-90–1	136.1	–9.4	–9.3	Calcite nodule	Doushantuo
16YJP-90–2	136.1	–5.4	–7.2	Argillaceous limestone	Doushantuo
16YJP-91	137	–1.3	–4.6	Argillaceous limestone	Doushantuo
16YJP-92	138	+0.5	–4.5	Argillaceous limestone	Doushantuo
16YJP-93–4	151.5	+0.0	–4.6	Limestone	Doushantuo
16YJP-93–1	151.5	–4.0	–7.5	Calcite nodule	Doushantuo
16YJP-93–2	151.5	–9.8	–11.2	Calcite nodule	Doushantuo
16YJP-93–3	151.5	–5.2	–12.8	Calcite nodule	Doushantuo
16YJP-94–2	153	+0.3	–3.5	Limestone	Doushantuo
16YJP-94–1	153	–11.4	–9.1	Calcite nodule	Doushantuo
16YJP-95	155	–1.8	–2.1	Limestone	Doushantuo
16YJP-96–3	156.5	–2.5	–4.4	Limestone	Doushantuo
16YJP-96–1	156.5	–15.2	–9.0	Calcite nodule	Doushantuo
16YJP-96–2	156.5	–18.6	–9.1	Calcite nodule	Doushantuo
16YJP-97	157	–8.8	–9.1	Limestone	Doushantuo
16YJP-98	160	–1.0	–2.4	Dolomite	Doushantuo
16YJP-99–3	161	–2.1	–5.2	Dolomite	Doushantuo
16YJP-99–1	161	–20.2	–9.1	Calcite nodule	Doushantuo
16YJP-99–2	161	–16.3	–8.7	Calcite nodule	Doushantuo
16YJP-100	161.5	–9.9	–8.8	Dolomite	Dengying
16YJP-101–4	162	–3.0	–6.7	Dolomite	Dengying
16YJP-101–1	162	–13.3	–10.0	Calcite nodule	Dengying
16YJP-101–2	162	–22.2	–9.5	Calcite nodule	Dengying
16YJP-101–3	162	–24.2	–9.6	Calcite nodule	Dengying
16YJP-102–4	162.1	–3.4	–6.2	Dolomite	Dengying
16YJP-102–1	162.1	–18.0	–9.7	Calcite nodule	Dengying
16YJP-102–2	162.1	–14.7	–9.1	Calcite nodule	Dengying
16YJP-102–3	162.1	–12.0	–9.0	Calcite nodule	Dengying
16YJP-103–3	162.3	–9.0	–8.5	Dolomite	Dengying
16YJP-103–1	162.3	–23.8	–10.4	Calcite nodule	Dengying
16YJP-103–2	162.3	–17.2	–8.9	Calcite nodule	Dengying
16YJP-104	163.5	+5.5	–5.2	Dolomite	Dengying
16YJP-105–1	164.5	+2.1	–6.2	Dolomite	Dengying
16YJP-105–2	164.5	–28.7	–9.6	Calcite nodule	Dengying
16YJP-106	165.5	+1.4	–6.4	Dolomite	Dengying
16YJP-107–1	166.4	–26.0	–9.1	Calcite nodule	Dengying
16YJP-108–2	167	–30.4	–9.9	Calcite nodule	Dengying
16YJP-110–2	167.7	+4.9	–5.5	Dolomite	Dengying
16YJP-110–1	167.7	–3.7	–10.1	Calcite nodule	Dengying
16YJP-110–3	167.7	–1.6	–5.3	Argillaceous dolomite	Dengying
16YJP-109–2	168.5	–10.4	–10.2	Dolomite	Dengying
16YJP-111–2	170.5	–5.7	–5.2	Dolomite	Dengying
16YJP-111–1	170.5	–18.8	–9.2	Calcite nodule	Dengying
16YJP-112–2	171.5	–2.2	–5.8	Dolomite	Dengying
16YJP-112–1	171.5	–26.3	–9.6	Calcite nodule	Dengying

(*continued on next page*)

Table 2 (*continued*)

Sample	Stratigraphic height(m)	$\delta^{13}C_{carb}$ (‰)	$\delta^{18}O_{carb}$ (‰)	Lithology	Formation
16YJP-113–1	173.4	–22.4	–9.5	Calcite nodule	Dengying
16YJP-114–1	173.6	–2.3	–8.6	Calcite nodule	Dengying
16YJP-114–2	173.6	+1.3	–4.7	Argillaceous dolomite	Dengying
16YJP-115–1	176.1	–24.1	–11.1	Calcite nodule	Dengying
16YJP-115–2	176.1	–2.1	–9.0	Argillaceous dolomite	Dengying
16YJP-116–1	178	–0.4	–6.1	Dolomite	Dengying
16YJP-117	179	+1.7	–6.3	Dolomite	Dengying
16YJP-118–2	179.9	–5.9	–7.9	Dolomite	Dengying
16YJP-118–1	179.9	–31.6	–9.5	Calcite nodule	Dengying
16YJP-119–2	181.7	–14.4	–9.7	Dolomite	Dengying
16YJP-119–1	181.7	–33.6	–9.7	Calcite nodule	Dengying
16YJP-120–2	183.4	+5.2	–4.0	Dolomite	Dengying
16YJP-120–1	183.4	–4.7	–10.7	Calcite nodule	Dengying
16YJP-121–2	185.8	+1.1	–2.6	Dolomite	Dengying
16YJP-121–1	185.8	–29.1	–9.1	Calcite nodule	Dengying
16YJP-122–2	187	–1.2	–4.6	Dolomite	Dengying
16YJP-122–1	187	–28.3	–10.2	Calcite nodule	Dengying
16YJP-123–1	188.9	–1.5	–4.9	Dolomite	Dengying
16YJP-123–2	188.9	–18.7	–9.9	Calcite nodule	Dengying
16YJP-123–3	188.9	–18.3	–10.0	Calcite nodule	Dengying
16YJP-124–3	191.1	–0.4	–5.6	Dolomite	Dengying
16YJP-124–1	191.1	–30.2	–9.5	Calcite nodule	Dengying
16YJP-125–1	194.3	+5.8	–4.3	Dolomite	Dengying
16YJP-125–2	194.3	+7.5	–2.7	Dolomite	Dengying
16YJP-125–3	194.3	–15.5	–10.3	Calcite nodule	Dengying
16YJP-126–1	196.7	+5.5	–3.9	Dolomite	Dengying
16YJP-126–2	196.7	+5.7	–3.3	Dolomite	Dengying
16YJP-126–3	196.7	+6.6	–3.4	Dolomite	Dengying
16YJP-126–4	196.7	–16.1	–10.2	Calcite nodule	Dengying
16YJP-127–4	197.3	+2.2	–4.9	Dolomite	Dengying
16YJP-127–5	197.3	+1.9	–4.5	Dolomite	Dengying
16YJP-127–1	197.3	–10.3	–10.1	Calcite nodule	Dengying
16YJP-127–2	197.3	–30.8	–10.7	Calcite nodule	Dengying
16YJP-127–3	197.3	–27.9	–10.8	Calcite nodule	Dengying
16YJP-127–6	197.3	–30.8	–11.5	Calcite nodule	Dengying
16YJP-128–1	197.9	+5.7	–3.3	Dolomite	Dengying
16YJP-128–2	197.9	–21.0	–9.9	Calcite nodule	Dengying
16YJP-128–3	197.9	–18.8	–10.5	Calcite nodule	Dengying
16YJP-129–1	199.8	+4.6	–4.1	Dolomite	Dengying
16YJP-130–1	200	+3.0	–4.4	Dolomite	Dengying
16YJP-130–2	200	–25.7	–11.1	Calcite nodule	Dengying
16YJP-130–3	200	–19.8	–11.0	Calcite nodule	Dengying
16YJP-131–1	202	+4.4	–4.7	Dolomite	Dengying
16YJP-131–2	202	–9.6	–10.3	Calcite nodule	Dengying
16YJP-131–3	202	–14.9	–9.7	Calcite nodule	Dengying
16YJP-132	205	+5.6	–5.8	Dolomite	Dengying
16YJP-133–1	206.8	+6.8	–5.8	Dolomite	Dengying
16YJP-134	209.3	+7.6	–4.1	Dolomite	Dengying
16YJP-135	212	+6.2	–5.2	Dolomite	Dengying
16YJP-136	214	+6.3	–5.0	Dolomite	Dengying
16YJP-137	216.5	+5.5	–5.2	Dolomite	Dengying
16YJP-138	218.7	+3.2	–5.1	Dolomite	Dengying
16YJP-139	220.5	+4.1	–2.9	Dolomite	Dengying
16YJP-140	222.1	+5.1	–3.0	Dolomite	Dengying
16YJP-141–1	223.2	+5.4	–3.6	Dolomite	Dengying
16YJP-141–2	223.2	+5.8	–3.0	Dolomite	Dengying
16YJP-142	225.4	+4.0	–3.2	Dolomite	Dengying
16YJP-143	226.5	+4.3	–3.5	Dolomite	Dengying
16YJP-144	229.3	+4.7	–4.5	Dolomite	Dengying
16YJP-145	232.1	+4.8	–2.8	Dolomite	Dengying
16YJP-146	234	+4.6	–3.2	Dolomite	Dengying
16YJP-147	236.1	+3.5	–4.0	Dolomite	Dengying
16YJP-148	240	+3.3	–5.1	Dolomite	Dengying

* Stratigraphic height is measured from an arbitrary datum (0 m) at ca. 161 m below the boundary between the Doushantuo and Dengying formations. Suffices denote different analyses for samples with replicate analyses and are not related to lithology of the sample.

and their $\delta^{18}O$ values fluctuate around − 9‰.

$\delta^{13}C$ profile of the Yangjiaping section is illustrated in Fig. 5, and detailed $\delta^{13}C$ and $\delta^{18}O$ data are presented in Table 2. The $\delta^{13}C$ values for the lower part of the carbonate interval (0–120 m) are mostly around + 5‰, except several samples in the lowermost part yielding values around 0‰ and a slightly negative shift at ca. 100 m. $\delta^{13}C$ values of the carbonate matrix from the transitional interval between the Doushantuo and Dengying formations (120–200 m), where calcite nodules mainly occur, vary between − 10‰ and + 10‰ (Fig. 5). Above the calcite nodule-bearing interval, $\delta^{13}C$ values show consistently positive values around + 5‰. The $\delta^{13}C$ values of calcite nodules at the Yangjiaping section also reveal strong variation, ranging from − 33.6‰ to − 2.2‰.

4.2. Silicified microfossils

Silicified microfossils have been recovered from cherty nodule samples in both the upper and lower intervals. The five cherty nodule samples from strata below and near the zero datum contain large amounts of recrystallized quartz minerals, and only yield rare, poorly-preserved filaments and leiospheres. Five out of the six cherty nodule samples (21DC-2 to 21DC-6) in the upper part of the carbonate interval (from 45 m to 50 m) yield abundant microfossils including filaments, sphaeromorphs, acanthomorphic acritarchs, and tubular microfossils (Figs. 2, 6–10). Preservation of many microfossils was strongly influenced by recrystallization of micro-quartz and calcite, but some microfossils are fairly well-preserved, allowing for taxonomic identification at least to the genus level.

Filaments of *Siphonophycus* (Fig. 6A, B) have been recovered from all five fossiliferous cherty nodule samples from the upper carbonate interval, representing the only prokaryotic fossil group at the Caojunba section. Fragments of microbial mats consisting of *Siphonophycus* filaments were found from a few thin sections, but in most cases these filaments only occur as disaggregated or clustered individuals.

Sphaeromorphic acritarchs are represented by *Leiosphaeridia tenuissima* of various size (Fig. 6C, D) at the Caojunba section. They occur abundantly in almost all thin sections of the five fossiliferous cherty nodule samples from the upper carbonate interval. They commonly form clusters consisting of tens of spheroids with similar or different sizes. There are also clusters of spheroidal acritarchs that bear possible ornamentations on their vesicles (Fig. 6E–G), but these possible ornamentations are too poorly-preserved to be confirmed as biogenic in origin.

Three tubular microfossil specimens of *Sinocyclocyclicus guizhouensis* (Fig. 6H) occur in the uppermost fossiliferous cherty nodule sample 21DC-2. Tubes of the three specimens are all incomplete, but similar in length, diameter, and orientation.

Acanthomorphic acritarchs also occur at all five fossiliferous horizons from the upper carbonate interval (Appendix table 1). Despite ornamentation in most specimens being partially destroyed by recrystallization, nine genera and eighteen species have been identified based on 88 fairly well-preserved specimens (Figs. 7–10). These taxa include *Appendisphaera grandis* (Fig. 7A, B), *Cavaspina acuminata* (Fig. 7C–E), *Cavaspina* cf. *C. basiconica* (Fig. 7F–H), *C. uria* (Fig. 7I–M), *Eotylotopalla dactylos* (Fig. 8A), *Eotylotopalla* cf. *E. dactylos* (Fig. 8B, differentiated from *E. dactylos* by its truncated process terminations), *Hocosphaeridium anozos* (Fig. 8G–K), *H. scaberfacium* (Fig. 8L, M), *Knollisphaeridium maximum* (Fig. 9A–C), *Mengeosphaera minima* (Fig. 8C), *M. minima*? (Fig. 8D, differentiated from *M. minima* by their densely arranged processes with inflated basal expansions), *Mengeosphaera* sp. (Fig. 8E, F), *Tanarium* cf. *T. capitatum* (Fig. 8N, O), *T. conoideum* (Fig. 9D, E), ?*T. pilosiusculum* (Fig. 9F, G), *T. tuberosum* (Fig. 9H), *Tanarium* sp. indet., ?*Verrucosphaera* sp. (Fig. 10A–F), *Weissiella* cf. *W. grandistella* (Fig. 10G–I). Whereas most of these taxa are represented by only one or a few specimens, ?*Verrucosphaera* sp. and *H. anozos* are quite abundant, making up 32% and 20% of all 98 acanthomorphic specimens, respectively.

5. Discussion

5.1. Correlation of the Doushantuo Formation in shelf-margin facies

The lithostratigraphic sequence and carbon isotopic profile of the Doushantuo Formation at Caojunba can be readily correlated with those of other shelf-margin sections such as the Yangjiaping and Zhongling sections. At these three sections, the Doushantuo Formation can be subdivided into a lower argillaceous interval with fine horizontal laminations, and an upper interval dominated by carbonate rocks that contain intraclastic and pisolitic beds indicative of high-energy shallow water environment. Calcite nodules are common in the upper carbonate rock interval in the shelf-margin area (Cui et al., 2016, 2017). The $\delta^{13}C$ profile at Caojunba also resembles those at Yangjiaping and Zhongling (Fig. 5). For carbonate rocks below the calcite nodule-bearing interval, $\delta^{13}C$ values are largely characterized by consistently positive $\delta^{13}C$ values (mean= +2.8‰ and s.d. = 3.0‰ for Caojunba; mean= +4.9‰ and s.d. = 2.2‰ for Yangjiaping), whereas in the calcite nodule-bearing interval, $\delta^{13}C$ values of dolomicrites generally show greater variations around 0‰, especially at the Caojunba and Yangjiaping sections (mean= +0.6‰ and s.d. = 4.4‰ for Caojunba; mean = − 0.6‰ and s.d. = 4.8‰ for Yangjiaping).

The Doushantuo Formation in the shelf-margin area has been correlated with the Doushantuo Formation in the Yangtze Gorges area (e.g., Zhu et al., 2007; Ader et al., 2009), despite a possible stratigraphic gap in the uppermost part in the shelf-margin area (Cui et al., 2015). In this correlation scheme, the lower argillaceous interval and the upper carbonate interval of the Doushantuo Formation in shelf-margin facies were correlated with Member II and Member III of the Doushantuo Formation in the Yangtze Gorges area, respectively. This correlation is consistent with the two-stage depositional evolution model of the Doushantuo Formation (Vernhet and Reijmer, 2010; Jiang et al., 2011). Accordingly, the negative $\delta^{13}C$ values in the upper part of the Doushantuo Formation and basal Dengying Formation at the Yangjiaping and Zhongling sections in the shelf-margin facies were correlated with EN3/Shuram excursion in the Yangtze Gorges area (Zhu et al., 2007; Jiang et al., 2011). Similarly, the Doushantuo Formation at Caojunba is also lithostratigraphically bipartite, and the negative $\delta^{13}C$ values in the upper part of the Doushantuo Formation could also be correlated with EN3.

Alternatively, Furuyama et al. (2016) correlated the negative $\delta^{13}C$ values in the upper Doushantuo Formation in shelf-margin facies with EN2 in the Yangtze Gorges area, and they further suggested the presence of a much longer stratigraphic gap in the upper Doushantuo Formation at the Yangjiaping section than was envisioned by Cui et al. (2015). This correlation was based on the elevated $^{87}Sr/^{86}Sr$ values (ca. 0.7085) within the upper Doushantuo negative $\delta^{13}C$ excursion interval at the Yangjiaping section (Cui et al., 2015; Furuyama et al., 2016), which are less radiogenic than those of the EN3 interval (ca., 0.7090, Jiang et al., 2007; Sawaki et al., 2010) and resemble those of the EN2 interval (Sawaki et al., 2010) in the Yangtze Gorges area. However, the $^{87}Sr/^{86}Sr$ values of the EN2 interval were obtained from argillaceous dolostone samples that can be easily contaminated by siliciclasts during sample preparation (Cui et al., 2016; Xiao et al., 2016). Indeed, when $^{87}Sr/^{86}Sr$ data are screened using [Sr] and carbonate contents, a $^{87}Sr/^{86}Sr$ peak of 0.7085–0.7090 corresponds to the Shuram excursion (Cui et al., 2020; Xiao and Narbonne, 2020). Therefore, the correlation proposed by Furuyama et al. (2016) is not followed in this study, and its veracity requires additional tests using independent stratigraphic data or radioisotopic ages.

Biostratigraphic data from the Caojunba section provide another line of evidence to test stratigraphic correlations between the carbonate intervals of the Doushantuo Formation in the shelf-margin facies and Member III in the Yangtze Gorges area. In the Yangtze Gorges area, different stratigraphic intervals of the Doushantuo Formation yield distinct microfossil compositions (e.g., Zhou et al., 2007; McFadden

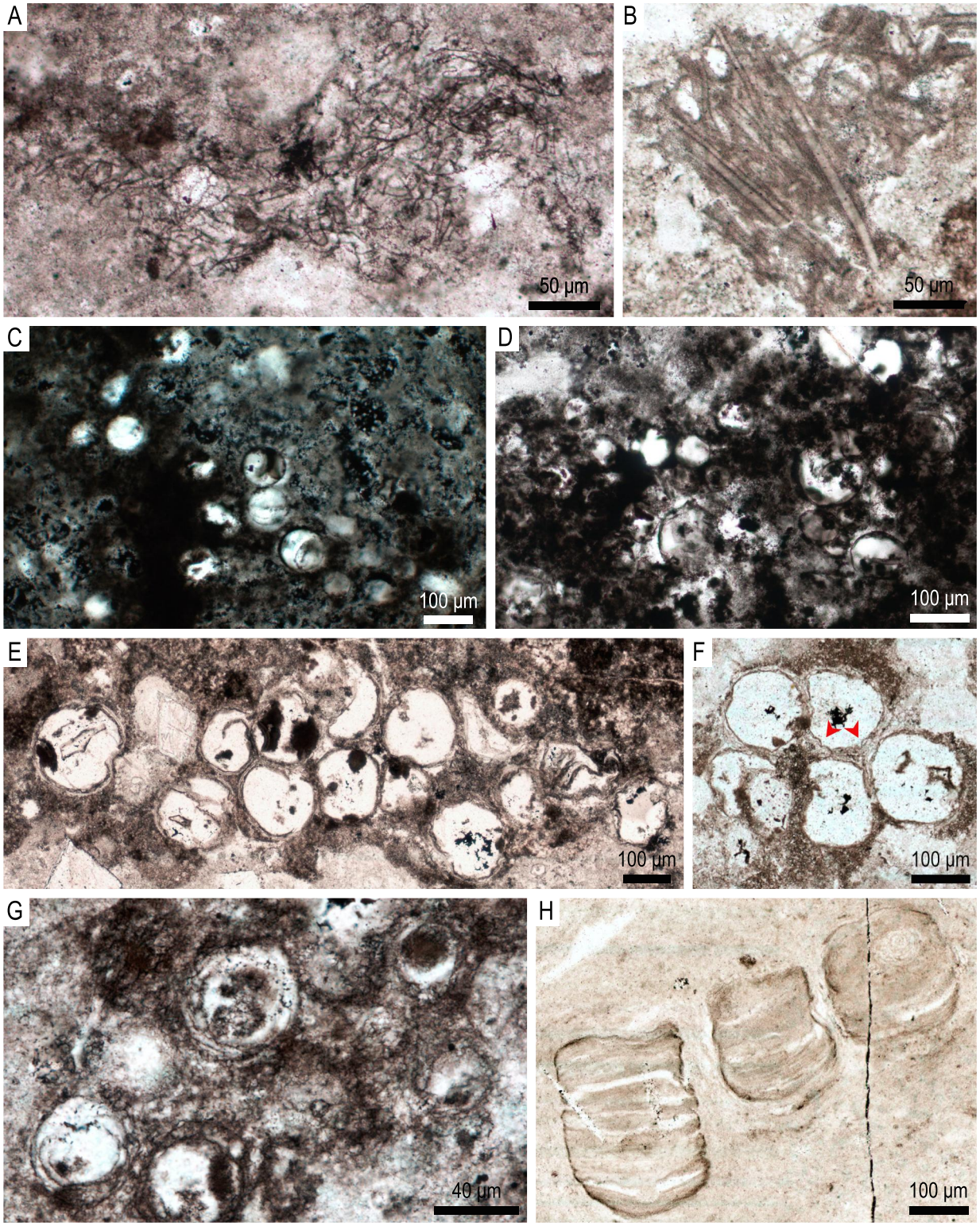

Fig. 6. Silicified microfossils from cherty nodules in the upper part of the Doushantuo Formation at the Caojunba section. England finder coordinates are given for specimens illustrated in this and the following figures. (A) *Siphonophycus septatum* (Schopf, 1968) Knoll et al., 1991. Thin section # 21DC-2–30, S42/2. (B) *Siphonophycus typicum* (Hermann, 1974) Butterfield in Butterfield et al., 1994. Thin section # 21DC-5–3, L44/2. (C)–(D) *Leiosphaeridia tenuissima* Eisenack, 1958. (C) Thin section # 21DC-2–17, B29/2. (D) Thin section # 21DC-2–27, K30/3. (E)–(G) Clusters of poorly-preserved but possibly ornamented acritarchs. (E) and (G) Thin section # 21DC-5–4, (E) O43/1, (G) Q40. (F) Thin section # 21DC-5–3, J35/2. Red arrowheads in (F) denote possible ornamentations. (H) *Sinocyclocyclicus guizhouensis* Xue et al., 1992 emend. Liu et al., 2008. Thin section # 21DC-2–36, L40/2.

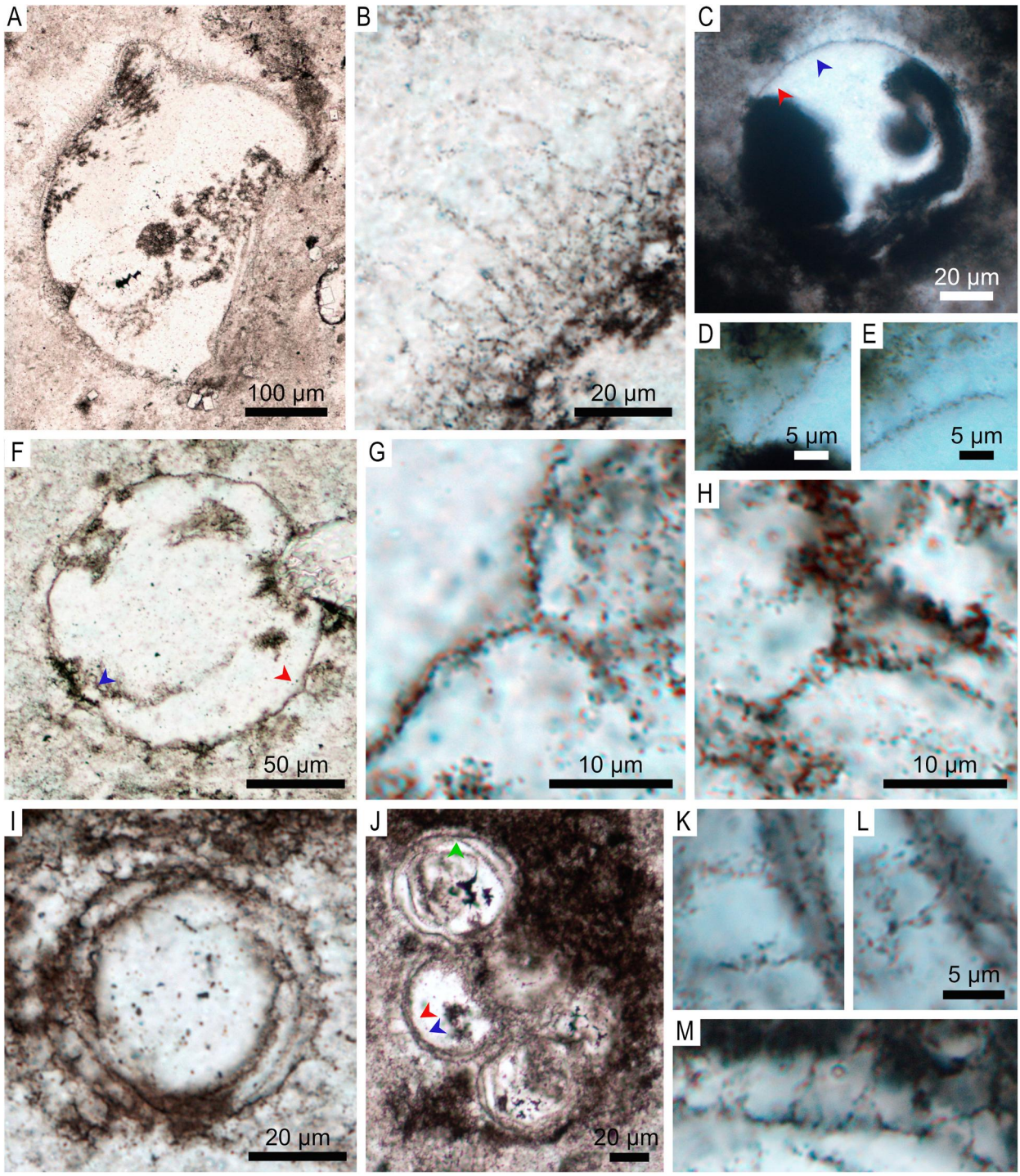

Fig. 7. Silicified microfossils from cherty nodules in the upper part of the Doushantuo Formation at the Caojunba section. (A)–(B) *Appendisphaera grandis* Moczydłowska et al., 1993 emend. Moczydłowska, 2005. Thin section 21DC-5–4, V34/1. (C)–(E) *Cavaspina acuminata* (Kolosova, 1991) Moczydłowska et al., 1993. Thin section 21DC-3–1, Q30/4. (D)–(E) Magnification of processes denoted by the red and blue arrowheads in (C), respectively. (F)–(H) *Cavaspina* cf. *C. basiconica*. Thin section 21DC-5–4, M40. (G)–(H) Magnification of the basally expanded processes denoted by red and blue arrowheads in (F). (I)–(M) *C. uria* (Nagovitsin and Faizullin in Nagovitsin et al., 2004) Nagovitsin and Moczydłowska in Moczydłowska and Nagovitsin, 2012. Thin section 21DC-5–4, (I) G41/1, (J)–(M) E45/4. (K)–(M) Magnification of conical processes denoted by red, blue, and green arrowheads in (J), respectively.

et al., 2009; Liu et al., 2013; Ouyang et al., 2021), forming the foundation of biostratigraphic correlation. Among all the stratigraphic intervals, the upper Doushantuo Formation (Member III) in the Yangtze Gorges area is characterized by microfossils with 1) diverse acanthomorphs of various sizes and ornamentations, 2) abundant occurrence of *Hocosphaeridium* species and *Tanarium conoideum*, and 3) clusters of small to medium-sized sphaeromorphs (Yin et al., 2011a; Liu et al., 2013, 2014a, 2014b). Recently, Liu and Moczydłowska (2019) also reported that *Knollisphaeridium maximum* occurs consistently and abundantly in Member III at several sections in the Yangtze Gorges area. The microfossil assemblage at Caojunba contains *H. scaberfacium*, *K. maximum*, *T. conoideum*, abundant *H. anozos*, and clusters of sphaeromorphs, similar to the Member III fossil assemblage in the Yangtze Gorges area in overall taxonomic composition and relative abundance.

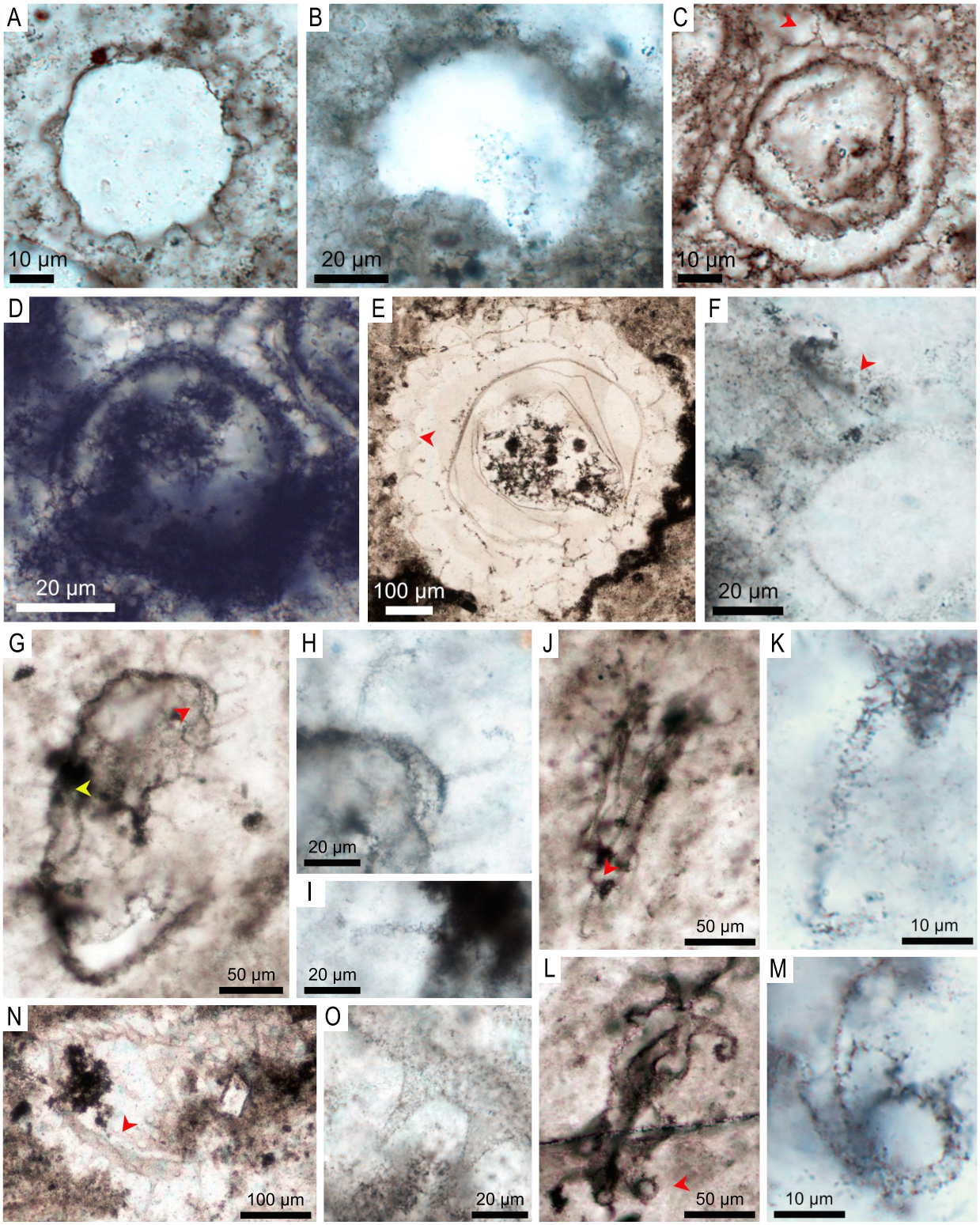

Fig. 8. Silicified microfossils from cherty nodules in the upper part of the Doushantuo Formation at the Caojunba section. (A) *Eotylotopalla dactylos* Zhang et al., 1998. Thin section 21DC-5–3, Q30/4. (B) *Eotylotopalla* cf. *E. dactylos*. Thin section 21DC-2–12, O21/2. (C) *Mengeosphaera minima* Liu et al., 2014b. Thin section 21DC-5–4, T31/2. Red arrowhead denotes a biform process with obtusely conical base and a thin apical spine. (D) *M. minima*? Thin section 21DC-3–1, G23/3. (E)–(F) *Mengeosphaera* sp. Thin section 21DC-2–35, P34/1. (F) Magnification of a biform process, with the reflection point denoted by a red arrowhead in (E). (G)–(K) *Hocosphaeridium anozos* (Willman in Willman and Moczydłowska, 2008) Xiao et al., 2014. Thin section 21DC-2–20, (G)–(I) O17/4, (J)–(K) P18/3. (H)–(I) Magnified view of the terminally hooked cylindrical processes denoted by red and yellow arrowheads in (G), respectively. (K) Magnified view of the terminally hooked process denoted by a red arrowhead in (J). (L)–(M) *H. scaberfacium* Zang in Zang and Walter, 1992. Thin section 21DC-2–20, O20/1. (M) Magnified view of the terminally hooked conical process denoted by a red arrowhead in (L). (N)–(O) *Tanarium* cf. *T. capitatum*. Thin section 21DC-2–35, M32/1. (O) Magnified view of processed denoted by a red arrowhead in (N).

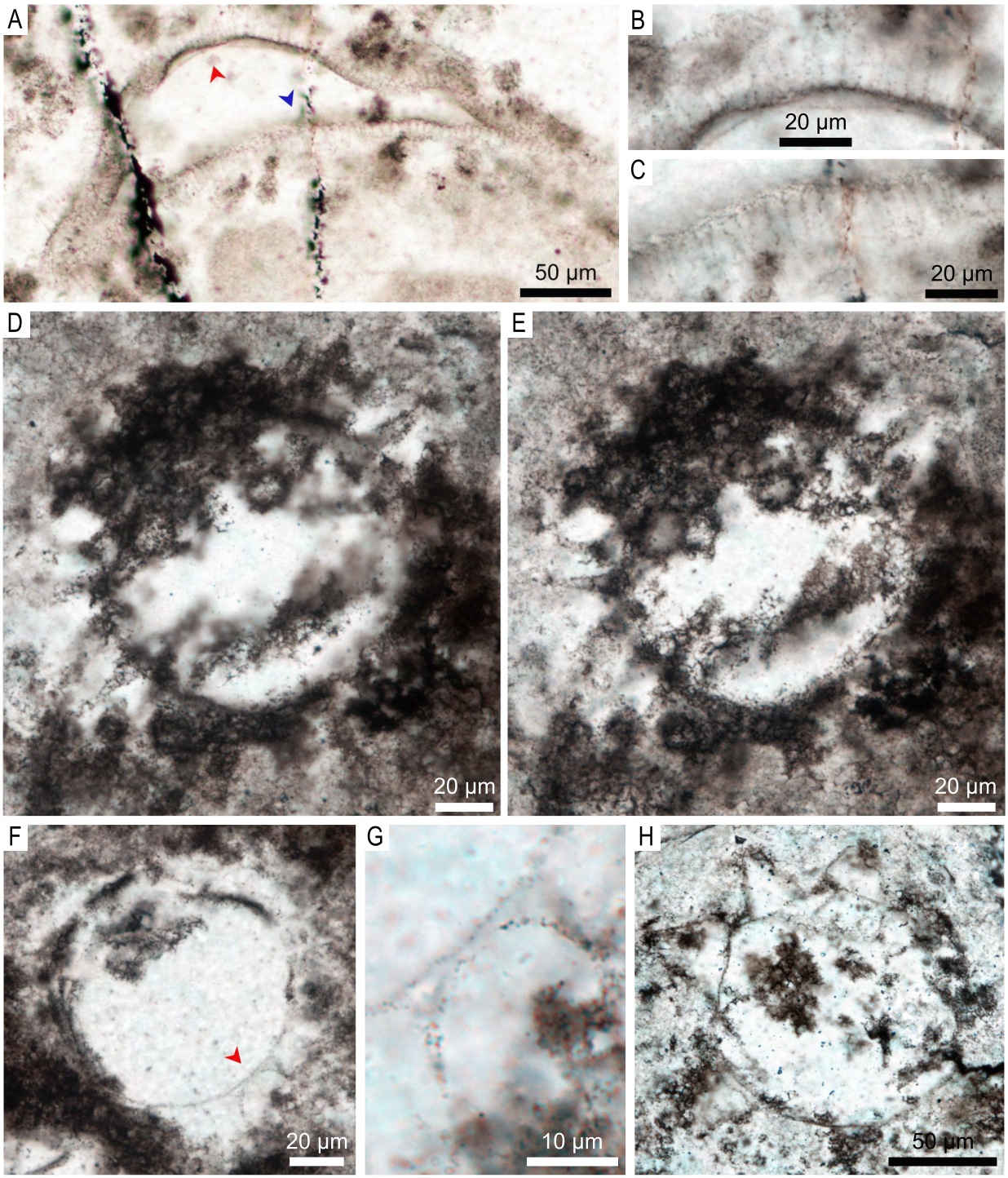

Fig. 9. Silicified microfossils from cherty nodules in the upper part of the Doushantuo Formation at the Caojunba section. (A)–(C) *Knollisphaeridium maximum* (Yin, 1987) Willman and Moczydłowska, 2008. Thin section 21DC-6–9, H34/4. (B)–(C) Magnified views of conical processes denoted by red and blue arrowheads in (A), respectively. (D)–(E) *Tanarium conoideum* Kolosova, 1991 emend. Moczydłowska et al., 1993, same specimen at different focal levels. Thin section 21DC-5–4, R43/3. (F)–(G) ?*T. pilosiusculum* Vorob'eva et al., 2009. Thin section 21DC-5–4, K45/4. (G) Magnified view of the two relatively short conical processes denoted by the red arrowhead in (F). (H) *T. tuberosum* Moczydłowska et al., 1993. Thin section 21DC-4–11, U45.

Although these taxa also occur occasionally in Member II in the Yangtze Gorges area or equivalent strata elsewhere (e.g., Hawkins et al., 2017; Liu and Moczydłowska, 2019; Liu et al., 2021), the above listed characteristics have been widely and consistently recognized from Member III, and thus are typical of Member III of the Doushantuo Formation. For example, *H. anozos* occurs rarely in Member II of the Doushantuo Formation in the Yangtze Gorges area (only two poorly-preserved specimens documented from Member II at the Niuping section, Liu and Moczydłowska, 2019), but it is abundant and widely distributed in Member III at numerous sections (present at six sections and common/abundant at four out of the seven Member III sections investigated by Liu and Moczydłowska, 2019). Thus, the abundant occurrence of *H. anozos* more likely indicates a correlation with Member III. Accepting the correlation between the Caojunba microfossil assemblage and the Member

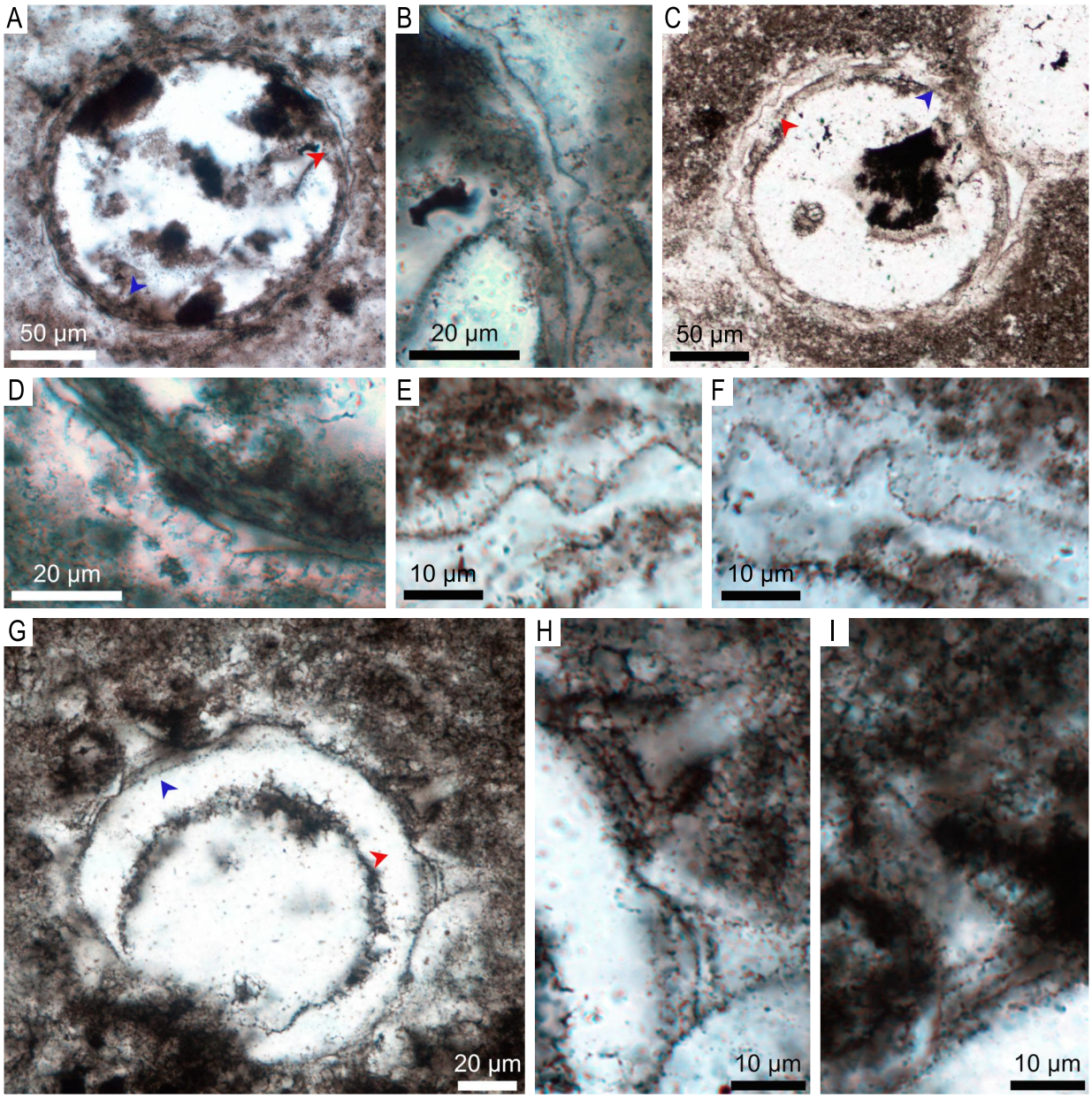

Fig. 10. Silicified microfossils from cherty nodules in the upper part of the Doushantuo Formation at the Caojunba section. (A)–(F) ?*Verrucosphaera* sp. (A), (B), and (D) Thin section 21DC-6–1, H44. (B) and (D) Magnified view of conical and hair-like processes denoted by red and blue arrowheads in (A), respectively. (C), (E), and (F) Thin section 21DC-5–3, P35/2. (E)–(F) Magnified views of conical and hair-like processes denoted by red and blue arrowheads in (C), respectively. (G)–(I) *Weissiella* cf. *W. grandistella*. Thin section 21DC-2–30, T35/1. (H)–(I) Magnification of conical processes with cross-walls denoted by red and blue arrowheads in (G), respectively.

III microfossil assemblage in the Yangtze Gorges area which corresponds to the stratigraphic interval of EP2–EN3 in Zhou and Xiao (2007), the interval yielding the distinct calcite nodules and fluctuating carbon isotopic data that coincides with the uppermost fossiliferous horizon at Caojunba (as well as its counterparts at Yangjiaping and Zhongling) is likely time-equivalent to EN3 rather than EN2 in the Yangtze Gorges area (Figs. 5, 11).

One potential problem with the correlation between the acanthomorphic assemblage at Caojunba and the Member III microfossil assemblage in the Yangtze Gorges area is the absence of *Tanarium pycnacanthum* and *Ceratosphaeridium glaberosum* in the Caojunba assemblage, both of which are eponymous species of a biozone proposed for Member III in the Yangtze Gorges area (Liu and Moczydłowska, 2019). However, these two species are actually not common in the upper Doushantuo Formation, as they have only been recorded at two out of the seven Member III sections in the Yangtze Gorges area (Liu and Moczydłowska, 2019). Thus, the absence of these two species is likely due to their rarity in the upper Doushantuo Formation.

The litho-, chemo-, and biostratigraphic data presented here consistently support the correlation of the carbonate interval of the upper Doushantuo Formation in the shelf-margin area with Member III in the shelf-lagoon Yangtze Gorges area. This correlation weakens the basis for a large stratigraphic gap in the upper Doushantuo Formation in the shelf-margin, which was based on the absence of EN3 and strata equivalent to Member III at the Yangjiaping section (Furuyama et al., 2016), although small-scale stratigraphic gaps may be present and the lithostratigraphic boundary between the Doushantuo and Dengying formations in different facies may be diachronous (Cui et al., 2015). The

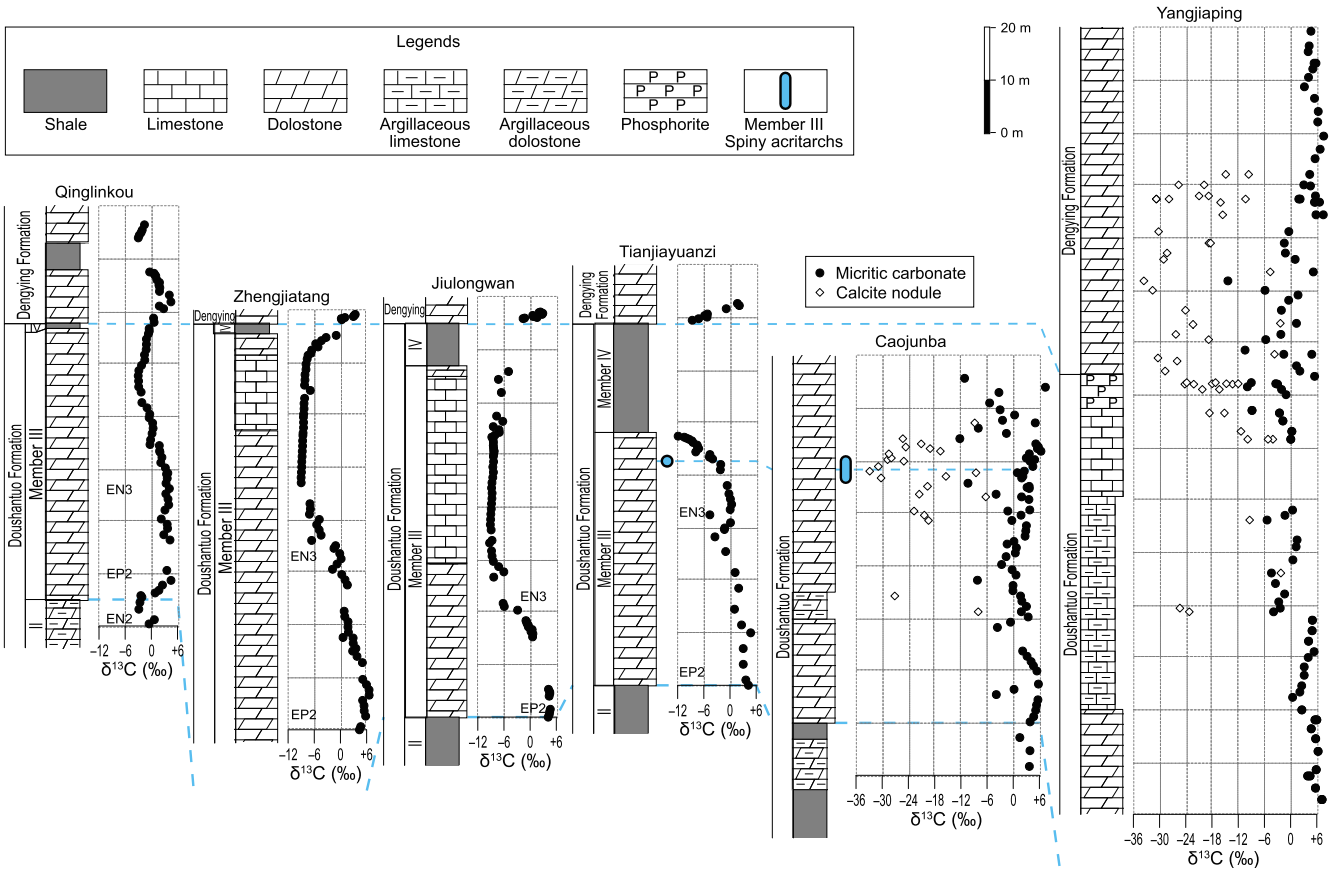

Fig. 11. Lithostratigraphic sequence and carbon isotopic profiles of the EN3 interval at selected sections in South China. Lithologies of each stratigraphic interval are simplified to represent only major lithological changes. Chemostratigraphic data sources: Qinglinkou, Zhengjiatang, Jiulongwan, and Tianjiayuanzi sections, Zhou et al. (2017); Caojunba and Yangjiaping sections, this study. Microfossil occurrence data sources: Tianjiayuanzi, Zhou et al. (2007); Caojunba, this study. Blue dash lines denote presumed correlations.

spatial variations in carbon isotopic chemostratigraphy of the upper Doushantuo Formation also indicate that local sedimentological and diagenetic processes may have played a role in shaping the chemostratigraphic record — a point that is discussed in greater detail below.

5.2. Chemostratigraphic implications

Subdivision and correlation of Ediacaran strata rely heavily on carbon isotopic profiles (Xiao and Narbonne, 2020). Among all the regionally recorded Ediacaran $\delta^{13}C$ excursions, the Shuram excursion in the middle Ediacaran (574.0 ± 4.7 to 567.3 ± 3.0 Ma, Rooney et al., 2020) is perhaps the most promising chemostratigraphic marker. It is considered to be the most pronounced $\delta^{13}C$ negative excursion in Earth history (with a nadir of ca. − 12‰), to have a consistent stratigraphic expression (with $\delta^{13}C$ values dropping abruptly to the nadir and then rising gradually to background values), and to represent a globally synchronous event (Grotzinger et al., 2011). The equivalent of the Shuram excursion in South China, EN3 in the upper Doushantuo Formation in the Yangtze Gorges area, is best represented at the Jiulongwan section, where $\delta^{13}C$ values reach the nadir of ca. − 10‰ in thin-bedded dolostone beds and then remain < − 8‰ through a 30-m-thick limestone interval (Jiang et al., 2007; McFadden et al., 2008).

Although EN3 has been recognized at multiple sections of the upper Doushantuo Formation in South China (Wang et al., 2011; Lu et al., 2013), there are some variations in stratigraphic range and magnitude of EN3 among different localities (Fig. 11). At the Zhengjiatang section to the northwest of Jiulongwan, the $\delta^{13}C$ curve of the EN3 interval largely resembles that at Jiulongwan, but differs from the latter in the preservation of a rising limb where $\delta^{13}C$ returns to positive values in topmost Member III carbonate rocks. At the Tianjiayuanzi section (the type section of the Doushantuo Formation) just ca. 6 km to the northeast of Jiulongwan, only the falling limb of EN3, which reaches a nadir of − 12‰, is recorded in the upper part of Member III carbonate rocks (Zhou et al., 2012; Lu et al., 2013). At the Qinglinkou section about 13 km to the west of Jiulongwan, a seemingly complete record of EN3 with both the falling and rising limbs is preserved in Member III dolostones, with a nadir of only ca. − 3‰ (An et al., 2015; Zhou et al., 2017). In the nearshore Lianghong section of western Yangtze block, the expression of EN3 resembles that at Qinglinkou, but with $\delta^{13}C$ values as low as − 8‰ (Wang et al., 2012), whereas at the more distal offshore Wangjiapeng section a negative $\delta^{13}C$ excursion tentatively correlated with EN3 has a stratigraphic thickness of < 10 m and a nadir of ca. − 6‰ (Lan et al., 2019). At the slope facies Siduping section, a negative $\delta^{13}C$ excursion at the top of the Doushantuo Formation shows a gradual decrease from ca. + 2‰ to ca. − 8‰, but the rising limb is not well-preserved due to the lack of carbonate rocks in the topmost Doushantuo Formation (similar to the case at Jiulongwan) and the overlying Liuchapo Formation (Wang et al., 2016). At the basinal facies Lantian section in southern Anhui Province, the expression of EN3 resembles that at the Jiulongwan section (Yuan et al., 2011; Wang et al., 2017a). The spatial variations in the chemostratigraphic expression of the EN3 interval is further evidenced by the highly variable $\delta^{13}C$ values in the upper Doushantuo Formation at Caojunba, Yangjiaping, and other shelf-margin sections.

One possible reason for the different expressions of the EN3/Shuram excursion in South China is the differential preservation of this excursion due to lithofacies change (e.g., carbonate vs. siliciclastic rocks) among different sections (Cui et al., 2016; Zhou et al., 2017; Lan et al., 2019). This is best demonstrated by the comparison of EN3 records at the

Tianjiayuanzi, Jiulongwan, and Zhengjiatang sections. The more carbonate strata in Member III of the Doushantuo Formation at these three sections, the more complete EN3 is preserved (Fig. 11; Zhou et al., 2017). However, differential preservation of EN3 cannot account for all observed variations. For example, complete EN3 profiles are recorded at both the Qinglinkou and Lianghong sections, but the magnitude of this excursion is much more subdued than at other sections. Another notable feature is that, in the shelf-margin facies (e.g., Yangjiaping, Zhongling, and Caojunba sections), the presumed EN3 in the upper Doushantuo Formation has highly variable $\delta^{13}C$ values (Fig. 5).

It is possible that the different expression of EN3 may be related to spatial heterogeneity of marine redox conditions during the Ediacaran Period as a result of ocean redox stratification (e.g., Jiang et al., 2007; Ader et al., 2009; Li et al., 2016; Husson et al., 2020; Wang et al., 2020; Cui et al., 2022). The Shuram excursion has been considered as a result of rising marine sulfate concentrations that led to the oxidation of a pre-existing pool of ^{13}C-depleted dissolved organic carbon in anoxic bottom waters below the marine chemocline (e.g., Fike et al., 2006; McFadden et al., 2008; Cui et al., 2017; Shields et al., 2019). Thus, carbonate rocks deposited in different localities below and above the chemocline may have different $\delta^{13}C$ values. EN3 sections located in the anoxic shelf-lagoon area, e.g., the Jiulongwan and Tianjiayuanzi sections, are characterized by a pronounced negative carbon isotopic excursion (McFadden et al., 2008; Zhou et al., 2012; Cui et al., 2021), whereas at shelf-margin sections such as the Yangjiaping, Zhongling, and Caojunba sections, which were probably located in oxic shallow water environments, highly variable $\delta^{13}C$ values are recorded in dolomicrite, along with extremely negative $\delta^{13}C$ values from calcite nodules (Fig. 5; Ader et al., 2009; Cui et al., 2017). The highly variable $\delta^{13}C$ values of dolomicrites from the EN3 interval at the shelf-margin sections may partly result from variable incorporation of authigenic calcite, which was derived from AOM and also gave rise to the calcite nodules with remarkably negative $\delta^{13}C$ values (Ader et al., 2009; Cui et al., 2017). In summary, the heterogeneous expressions of EN3 and correlative carbon isotopic records in different localities/facies of South China likely reflect different environmental conditions in a stratified Ediacaran ocean. These variations complicate chemostratigraphic correlations among sections from different depositional facies and highlight the importance of integrative stratigraphic correlation (Xiao et al., 2022).

5.3. Biostratigraphic implications

Although considered as a promising stratigraphic tool for the correlation of lower Ediacaran strata (Xiao et al., 2016, 2022), application of acritarch biozones to intra- and inter-basinal stratigraphic correlations has met with limited success (e.g., Grey, 2005; Liu and Moczydłowska, 2019; Xiao et al., 2022). In South China, several biozonation schemes have been proposed for the Doushantuo Formation, mainly based on presence/absence data of certain selected acritarch species in the Yangtze Gorges area (Liu et al., 2013; Xiao et al., 2014; Liu and Moczydłowska, 2019). The application of these acritarch biozones in regional and global correlations of Ediacaran successions is still in a nascent stage. However, the discovery of typical Member III microfossils from the shelf-margin Caojunba section sheds some light on this issue.

One major problem of the previously proposed biozones in the Doushantuo Formation is that the biozones are based exclusively on data from sections in the Yangtze Gorges area (McFadden et al., 2009; Liu et al., 2014b; Liu and Moczydłowska, 2019). At most sections outside the Yangtze Gorges area, only a small number of acritarch taxa were discovered from each section, not enough to fully document the diversity at these sections or the stratigraphic ranges of these taxa (Hawkins et al., 2017; Nie et al., 2017; Ouyang et al., 2017; Shang and Liu, 2020). At the Weng'an and Songlin areas where diverse and abundant acanthomorphs were reported, taxonomic compositions are somewhat different from those of the Doushantuo Formation in the Yangtze Gorges area (Xiao et al., 2014, and references therein; Shang et al., 2019).

The overall similarity between the acritarch assemblage at Caojunba and Member III microfossils in the Yangtze Gorges area indicates that at least certain taxa characteristic of the Member III acritarch assemblage recognized in the Yangtze Gorges area were distributed at a basinal scale, which serves as the biostratigraphic basis for our correlation in section 5.1. These taxa — including *Hocosphaeridium* species, *Knollisphaeridium maximum*, *Tanarium conoideum*, clustered sphaeromorphs, and likely some *Mengeosphaera* species as revealed by Liu et al. (2014b) — are here considered as typical Member III microfossils. Their relative abundance in the upper Doushantuo Formation may vary among localities due to the local dominance of other taxa (e.g., ?*Verrucosphaera* sp. at the Caojunba section), but these typical Member III taxa would be common if sampling intensity is adequate. At least, with sufficient sampling intensity (as the case in Caojunba), the typical Member III taxa should be encountered in the upper Doushantuo Formation at sections in shelf-margin and slope facies. This expectation is met in a biostratigraphic study of the upper slope Lujiayuanzi section in Hunan Province, where clusters of leiospheres are present and *K. maximum* occur as the most abundant acanthomorph taxon in the upper Doushantuo Formation (Ouyang et al., 2017).

More fossil data are needed to test whether characteristic Member II microfossils in shelf-lagoon facies also occur in the shelf-margin area. One of the most characteristic features of lower Member II microfossils in the Yangtze Gorges area is the occurrence of *Tianzhushania*, which is abundant and typically the most dominant genus in lower Member II at most fossiliferous sections (Liu and Moczydłowska, 2019; Ouyang et al., 2021). However, this genus has not yet been reported from the lower Doushantuo Formation in shelf-margin or slope facies, with the exception of the Weng'an area (Xiao et al., 2014), where the *Tianzhushania*-bearing strata was correlated with the upper Member II in the Yangtze Gorges area (Xiao et al., 2012, 2014; Ouyang et al., 2019). However, the Doushantuo Formation at Weng'an is much thinner than other localities, and high-resolution biostratigraphic data are thus far lacking. Considering that *Tianzhushania* has also been reported from the lower Ediacaran Infra-Krol Formation in Lesser Himalaya of northern India (Joshi and Tiwari, 2016), the absence of *Tianzhushania* in most shelf-margin and slope facies is likely a result of inadequate sampling, taphonomic artifact, or environmental constraints.

The upper Member II in the Yangtze Gorges area is characterized by a decline in the abundance of *Tianzhushania* and a rise of small spiny acritarchs such as *Dicrospinasphaera* species and *Ericiasphaera fibrilla* (Ouyang et al., 2021). Microfossil assemblages at Weng'an, Songlin, and Zhangcunping areas also share these features, as well as the emergence of some typical Member III taxa such as *Hocosphaeridium* species and *Tanarium conoideum* (Yin et al., 2011b; Xiao et al., 2014; Ouyang et al., 2019; Shang et al., 2019). This may indicate that the transition from lower Member II to the Member III fossil assemblages is gradual, as suggested by Xiao et al. (2012) and Xiao et al. (2014), with the typical lower Member II taxa gradually giving way to typical Member III taxa. Such a transition may occur asynchronously in a basinal scale, resulting in diachroneity in the first appearance and variations in the relative abundance of some species. If so, more nuanced details have to be taken into considerations when using Ediacaran acanthomorphs for high-resolution biostratigraphic correlation.

6. Conclusions

Integrated litho-, chemo-, and biostratigraphic data from the Caojunba section illustrate that the Doushantuo Formation in the shelf-margin facies of the Yangtze Block in South China, typically consisting of a lower argillaceous interval and an upper carbonate interval, is readily correlative with the Doushantuo Formation in the shelf-lagoon Yangtze Gorges area. The negative $\delta^{13}C$ excursion EN3 can be correlated with the upper Doushantuo Formation in shelf-margin facies, weakening the basis for a large-scale stratigraphic gap in the

Doushantuo Formation of the shelf-margin facies. Extremely negative $\delta^{13}C$ values of calcite nodules occur in the upper Doushantuo Formation (and lower Dengying Formation, e.g., at Yangjiaping section) in the shelf-margin facies may represent a regional biogeochemical event that is roughly contemporaneous with the $\delta^{13}C$ excursion EN3. Possibly owing to facies changes and different redox conditions, the expressions (e.g., stratigraphic thickness and magnitude) of EN3 can be highly variable across the Yangtze block of South China.

Diverse silicified microfossils including abundant acanthomorphic acritarch are for the first time reported from the shelf-margin facies in Hunan Province, expanding their spatial distribution in South China. These fossils from the upper carbonate interval at the Caojunba section reveal notable similarity, in both taxonomic diversity and relative abundance, to those from Member III of the Doushantuo Formation in the Yangtze Gorges area. This similarity affirms that certain features of the upper Doushantuo microfossil assemblage (e.g., occurrence of clustered leiosphere and abundance of *Hocosphaeridium* species) can be used for first-order biostratigraphic correlation at a basinal scale.

CRediT authorship contribution statement

Hongyi Shi: Investigation, Formal analysis, Writing – original draft. **Qing Ouyang:** Conceptualization, Investigation, Formal analysis, Writing – original draft, Writing – review & editing, Funding acquisition. **Chuanming Zhou:** Conceptualization, Investigation, Writing – review & editing, Supervision, Funding acquisition. **Shuhai Xiao:** Investigation, Writing – review & editing, Funding acquisition. **Zhe Chen:** Investigation. **Chengguo Guan:** Formal analysis, Writing – review & editing.

Declaration of Competing Interest

The authors declare that they have no known competing financial interests or personal relationships that could have appeared to influence the work reported in this paper.

Acknowledgements

This study was supported by the Strategic Priority Research Program (B) of Chinese Academy of Sciences (XDB26000000), National Natural Science Foundation of China (41902006, 41921002, and 41972005), the National Key R & D Program of China (2017YFC0603101), and State Key Laboratory of Biogeology and Environmental Geology (GBL22106). S. X. was supported by the National Science Foundation (EAR-2021207). We thank Yefei Shao for field and lab assistances, and two anonymous reviewers for constructive comments.

Appendix A. Supplementary data

Supplementary data to this article can be found online at https://doi.org/10.1016/j.precamres.2022.106699.

References

Ader, M., Macouin, M., Trindade, R.I.F., Hadrien, M.-H., Yang, Z., Sun, Z., Besse, J., 2009. A multilayered water column in the Ediacaran Yangtze platform? Insights from carbonate and organic matter paired $\delta^{13}C$. Earth Planet. Sci. Lett. 288 (1-2), 213–227.

An, Z., Jiang, G., Tong, J., Tian, L.i., Ye, Q., Song, H., Song, H., 2015. Stratigraphic position of the Ediacaran Miaohe biota and its constrains on the age of the upper Doushantuo δ13C anomaly in the Yangtze Gorges area, South China. Precambr. Res. 271, 243–253.

Butterfield, N.J., Knoll, A.H., Swett, K., 1994. Paleobiology of the Neoproterozoic Svanbergfjellet Formation, Spitsbergen. Fossils and Strata 34, 1–84.

Cao, R., Tang, T., Xue, Y., Yu, C., Yin, L., Zhao, W., 1989. Research on Sinian Strata with ore deposits in the Yangzi (Yangtze) Region, China, in: Nanjing Institute of Geology and Palaeontology, Chinese Academy of Sciences (Eds.), Upper Precambrian of the Yangzi (Yangtze) Region, China. Nanjing University Press, Nanjing, pp. 1–94.

Cui, H., Kaufman, A.J., Xiao, S., Zhou, C., Liu, X.-M., 2017. Was the Ediacaran Shuram Excursion a globally synchronized early diagenetic event? Insights from methane-derived authigenic carbonates in the uppermost Doushantuo Formation, South China. Chem. Geol. 450, 59–80.

Cui, H., Kaufman, A.J., Xiao, S., Zhu, M., Zhou, C., Liu, X.-M., 2015. Redox architecture of an Ediacaran ocean margin: integrated chemostratigraphic ($\delta^{13}C$–$\delta^{34}S$–$^{87}Sr/^{86}Sr$–Ce/Ce*) correlation of the Doushantuo Formation, South China. Chem. Geol. 405, 48–62.

Cui, H., Kaufman, A.J., Zou, H., Kattan, F.H., Trusler, P., Smith, J., Yu. Ivantsov, A., Rich, T.H., Al Qubsani, A., Yazedi, A., Liu, X.-M., Johnson, P., Goderis, S., Claeys, P., Vickers-Rich, P., 2020. Primary or secondary? A dichotomy of the strontium isotope anomalies in the Ediacaran carbonates of Saudi Arabia. Precambr. Res. 343, 105720. https://doi.org/10.1016/j.precamres.2020.105720.

Cui, H., Kitajima, K., Orland, I.J., Baele, J.-M., Xiao, S., Kaufman, A.J., Denny, A., Spicuzza, M.J., Fournelle, J.H., Valley, J.W., 2022. An authigenic response to Ediacaran surface oxidation: remarkable micron-scale isotopic heterogeneity revealed by SIMS. Precambr. Res. in press.

Cui, H., Kitajima, K., Orland, I.J., Xiao, S., Baele, J.-M., Kaufman, A.J., Denny, A., Zhou, C., Spicuzza, M.J., Fournelle, J.H., Valley, J.W., 2021. Deposition or diagenesis? Probing the Ediacaran Shuram excursion in South China by SIMS. Glob. Planet. Change 206, 103591. https://doi.org/10.1016/j.gloplacha.2021.103591.

Cui, H., Xiao, S., Zhou, C., Peng, Y., Kaufman, A.J., Plummer, R.E., 2016. Phosphogenesis associated with the Shuram Excursion: petrographic and geochemical observations from the Ediacaran Doushantuo Formation of South China. Sediment. Geol. 341, 134–146.

Eisenack, A., 1958. Mikroplankton aus dem norddeutschen Apt, nebst einigen Bemerkungen über fossile Dinoflagellaten. Neues Jahrbuch für Geologie und Paläontologie, Abhandlungen 106, 383–422.

Fan, H., Ostrander, C.M., Auro, M., Wen, H., Nielsen, S.G., 2021. Vanadium isotope evidence for expansive ocean euxinia during the appearance of early Ediacara biota. Earth Planet. Sci. Lett. 567, 117007. https://doi.org/10.1016/j.epsl.2021.117007.

Fike, D.A., Grotzinger, J.P., Pratt, L.M., Summons, R.E., 2006. Oxidation of the Ediacaran ocean. Nature 444 (7120), 744–747.

Furuyama, S., Kano, A., Kunimitsu, Y., Ishikawa, T., Wang, W., 2016. Diagenetic overprint to a negative carbon isotope anomaly associated with the Gaskiers glaciation of the Ediacaran Doushantuo Formation in South China. Precambr. Res. 276, 110–122.

Gan, T., Luo, T., Pang, K., Zhou, C., Zhou, G., Wan, B., Li, G., Yi, Q., Czaja, A.D., Xiao, S., 2021. Cryptic terrestrial fungus-like fossils of the early Ediacaran Period. Nat. Commun. 12, 641.

Grey, K., 2005. Ediacaran palynology of Australia. Association of Australasian Palaeontologists, Canberra.

Grotzinger, J.P., Fike, D.A., Fischer, W.W., 2011. Enigmatic origin of the largest-known carbon isotope excursion in Earth's history. Nat. Geosci. 4 (5), 285–292.

Guan, C., Zhou, C., Wang, W., Wan, B., Yuan, X., Chen, Z., 2014. Fluctuation of shelf basin redox conditions in the early Ediacaran: evidence from Lantian Formation black shales in South China. Precambr. Res. 245, 1–12.

Hawkins, A.D., Xiao, S., Jiang, G., Wang, X., Shi, X., 2017. New biostratigraphic and chemostratigraphic data from the Ediacaran Doushantuo Formation in intra-shelf and upper slope facies of the Yangtze platform: implications for biozonation of acanthomorphic acritarchs in South China. Precambr. Res. 300, 28–39.

Hermann, T.N., 1974. Findings of mass accumulations of trichomes in the Riphean. Proterozoic and Paleozoic microfossils of the U. S. S. R., Nauka, Moscow, pp. 6–10.

Husson, J.M., Linzmeier, B.J., Kitajima, K., Ishida, A., Maloof, A.C., Schoene, B., Peters, S.E., Valley, J.W., 2020. Large isotopic variability at the micron-scale in 'Shuram' excursion carbonates from South Australia. Earth Planet. Sci. Lett. 538, 116211. https://doi.org/10.1016/j.epsl.2020.116211.

Jiang, G., Kaufman, A.J., Christie-Blick, N., Zhang, S., Wu, H., 2007. Carbon isotope variability across the Ediacaran Yangtze platform in South China: implications for a large surface-to-deep ocean $\delta^{13}C$ gradient. Earth Planet. Sci. Lett. 261 (1-2), 303–320.

Jiang, G., Shi, X., Zhang, S., Wang, Y., Xiao, S., 2011. Stratigraphy and paleogeography of the Ediacaran Doushantuo Formation (ca. 635–551Ma) in South China. Gondwana Res. 19 (4), 831–849.

Joshi, H., Tiwari, M., 2016. *Tianzhushania spinosa* and other large acanthomorphic acritarchs of Ediacaran Period from the Infrakrol Formation, Lesser Himalaya. India. Precambr. Res. 286, 325–336.

Knoll, A., Walter, M., Narbonne, G.U.Y., Christie-Blick, N., 2006. The Ediacaran Period: a new addition to the geologic time scale. Lethaia 39, 13–30.

Knoll, A.H., Swett, K., Mark, J., 1991. Paleobiology of a Neoproterozoic Tidal Flat/Lagoonal Complex: The Draken Conglomerate Formation. Spitsbergen. J. Paleontol. 65 (4), 531–570.

Kolosova, S.P., 1991. Pozdnedokembriyskie shipovatie mikrofossilii vostoka sibirkoy platformi. Algologiya 1, 53–59.

Kunimitsu, Y., Setsuda, Y., Furuyama, S., Wang, W., Kano, A., 2011. Ediacaran chemostratigraphy and paleoceanography at a shallow marine setting in northwestern Hunan Province, South China. Precambr. Res. 191 (3-4), 194–208.

Lan, Z., Sano, Y., Yahagi, T., Tanaka, K., Shirai, K., Papineau, D., Sawaki, Y., Ohno, T., Abe, M., Yang, H., Liu, H., Jiang, T., Wang, T., 2019. An integrated chemostratigraphic ($\delta^{13}C$-$\delta^{18}O$-$^{87}Sr/^{86}Sr$-$\delta^{15}N$) study of the Doushantuo Formation in western Hubei Province, South China. Precambr. Res. 320, 232–252.

Li, C., Hardisty, D.S., Luo, G., Huang, J., Algeo, T.J., Cheng, M., Shi, W., An, Z., Tong, J., Xie, S., Jiao, N., Lyons, T.W., 2017. Uncovering the spatial heterogeneity of Ediacaran carbon cycling. Geobiology 15 (2), 211–224.

Liu, H., Qi, S., Fan, J., Guo, W., Pei, M., Huang, D., Cheng, L., Bian, M., Liu, L., Zhao, Y., Zhang, J., 2021. An acritarch assemblage from the lower Ediacaran Doushantuo Formation in Changyang, Hubei Province. Journal of Stratigraphy 45, 19–28.
Liu, P., Chen, S., Zhu, M., Li, M., Yin, C., Shang, X., 2014a. High-resolution biostratigraphic and chemostratigraphic data from the Chenjiayuanzi section of the Doushantuo Formation in the Yangtze Gorges area, South China: implication for subdivision and global correlation of the Ediacaran System. Precambr. Res. 249, 199–214.
Liu, P., Moczydłowska, M., 2019. Ediacaran microfossils from the Doushantuo Formation chert nodules in the Yangtze Gorges area, South China, and new biozones. Fossils and Strata 65, 1–172.
Liu, P., Xiao, S., Yin, C., Chen, S., Zhou, C., Li, M., 2014b. Ediacaran acanthomorphic acritarchs and other microfossils from chert nodules of the upper Doushantuo Formation in the Yangtze Gorges Area, South China. J. Paleontol. 88, 1–139.
Liu, P., Xiao, S., Yin, C., Zhou, C., Gao, L., Tang, F., 2008. Systematic description and phylogenetic affinity of tubular microfossils from the Ediacaran Doushantuo Formation at Weng'an, South China. Palaeontology 51, 339–366.
Liu, P., Yin, C., Chen, S., Tang, F., Gao, L., 2013. The biostratigraphic succession of acanthomorphic acritarchs of the Ediacaran Doushantuo Formation in the Yangtze Gorges area, South China and its biostratigraphic correlation with Australia. Precambr. Res. 225, 29–43.
Lu, M., Zhu, M., Zhang, J., Shields-Zhou, G., Li, G., Zhao, F., Zhao, X., Zhao, M., 2013. The DOUNCE event at the top of the Ediacaran Doushantuo Formation, South China: Broad stratigraphic occurrence and non-diagenetic origin. Precambr. Res. 225, 86–109.
McFadden, K.A., Huang, J., Chu, X., Jiang, G., Kaufman, A.J., Zhou, C., Yuan, X., Xiao, S., 2008. Pulsed oxidation and biological evolution in the Ediacaran Doushantuo Formation. Proc. Natl. Acad. Sci. 105, 3197–3202.
McFadden, K.A., Xiao, S., Zhou, C., Kowalewski, M., 2009. Quantitative evaluation of the biostratigraphic distribution of acanthomorphic acritarchs in the Ediacaran Doushantuo Formation in the Yangtze Gorges area, South China. Precambr. Res. 173, 170–190.
Moczydłowska, M., 2005. Taxonomic review of some Ediacaran acritarchs from the Siberian Platform. Precambr. Res. 136, 283–307.
Moczydłowska, M., Nagovitsin, K.E., 2012. Ediacaran radiation of organic-walled microbiota recorded in the Ura Formation, Patom Uplift, East Siberia. Precambr. Res. 198–199, 1–24.
Moczydłowska, M., Vidal, G., Rudavskaya, V.A., 1993. Neoproterozoic (Vendian) phytoplankton from the Siberian platform, Yakutia. Palaeontology 36, 495–521.
Muscente, A.D., Hawkins, A.D., Xiao, S., 2015. Fossil preservation through phosphatization and silicification in the Ediacaran Doushantuo Formation (South China): a comparative synthesis. Palaeogeogr. Palaeoclimatol. Palaeoecol. 434, 46–62.
Nagovitsin, K.E., Faizullin, M.S., Yakshin, M.S., 2004. New forms of Baikalian acanthomorphytes from the Ura Formation of the Patom Uplift, East Siberia. Geologiya e Geofisika 45, 7–19.
Narbonne, G.M., Xiao, S., Shields, G.A., Gehling, J.G., 2012. The Ediacaran Period. In: Gradstein, F.M., Ogg, J.G., Schmitz, M.D., Ogg, G.M. (Eds.), The Geologic Time Scale. Elsevier, Boston, pp. 413–435.
Nie, X., Liu, H., Dong, L., 2017. Ediacaran microfossils from the Doushantuo Formation of the Siduping section, Zhangjiajie, Hunan Province. China. Acta Micropalaeontol. Sin. 34, 369–389.
Ouyang, Q., Guan, C., Zhou, C., Xiao, S., 2017. Acanthomorphic acritarchs of the Doushantuo Formation from an upper slope section in northwestern Hunan Province, South China, with implications for early–middle Ediacaran biostratigraphy. Precambr. Res. 298, 512–529.
Ouyang, Q., Zhou, C., Xiao, S., Chen, Z., Shao, Y., 2019. Acanthomorphic acritarchs from the Ediacaran Doushantuo Formation at Zhangcunping in South China, with implications for the evolution of early Ediacaran eukaryotes. Precambr. Res. 320, 171–192.
Ouyang, Q., Zhou, C., Xiao, S., Guan, C., Chen, Z., Yuan, X., Sun, Y., 2021. Distribution of Ediacaran acanthomorphic acritarchs in the lower Doushantuo Formation of the Yangtze Gorges area, South China: evolutionary and stratigraphic implications. Precambr. Res. 353, 106005.
Rooney, A.D., Cantine, M.D., Bergmann, K.D., Gómez-Pérez, I., Al Baloushi, B., Boag, T. H., Busch, J.F., Sperling, E.A., Strauss, J.V., 2020. Calibrating the coevolution of Ediacaran life and environment. Proc. Natl. Acad. Sci. 117, 16824–16830.
Sawaki, Y., Ohno, T., Tahata, M., Komiya, T., Hirata, T., Maruyama, S., Windley, B.F., Han, J., Shu, D., Li, Y., 2010. The Ediacaran radiogenic Sr isotope excursion in the Doushantuo Formation in the Three Gorges area, South China. Precambr. Res. 176, 46–64.
Schopf, J.W., 1968. Microflora of the Bitter Springs Formation, Late Precambrian, Central Australia. J. Paleontol. 42, 651–688.
Shang, X., Liu, P., 2020. Acritarchs from the Ediacaran Doushantuo Formation at the Tianping section in Zhangjiajie area of Hunan Province, South China and their biostratigraphic significance. J. Stratigraphy 44, 150–162.
Shang, X., Liu, P., Moczydłowska, M., 2019. Acritarchs from the Doushantuo Formation at Liujing section in Songlin area of Guizhou Province, South China: implications for early–middle Ediacaran biostratigraphy. Precambr. Res. 334, 105453.
Shields, G.A., Mills, B.J.W., Zhu, M., Raub, T.D., Daines, S.J., Lenton, T.M., 2019. Unique Neoproterozoic carbon isotope excursions sustained by coupled evaporite dissolution and pyrite burial. Nat. Geosci. 12, 823–827.
Vernhet, E., Reijmer, J.J.G., 2010. Sedimentary evolution of the Ediacaran Yangtze platform shelf (Hubei and Hunan provinces, Central China). Sediment. Geol. 225, 99–115.
Vorob'eva, N.G., Sergeev, V.N., Knoll, A.H., 2009. Neoproterozoic microfossils from the northeastern margin of the East European Platform. J. Paleontol. 83, 161–196.
Wang, J., Li, Z., 2003. History of Neoproterozoic rift basins in South China: implications for Rodinia break-up. Precambr. Res. 122, 141–158.
Wang, W., Cawood, P.A., Pandit, M.K., Xia, X., Raveggi, M., Zhao, J., Zheng, J., Qi, L., 2021. Fragmentation of South China from greater India during the Rodinia-Gondwana transition. Geology 49, 228–232.
Wang, W., Guan, C., Hu, Y., Cui, H., Muscente, A.D., Chen, L., Zhou, C., 2020. Spatial and temporal evolution of Ediacaran carbon and sulfur cycles in the Lower Yangtze Block. South China. Palaeogeogr. Palaeoclimatol. Palaeoecol. 537, 109417.
Wang, W., Guan, C., Zhou, C., Peng, Y., Pratt, L.M., Chen, X., Chen, L., Chen, Z., Yuan, X., Xiao, S., 2017a. Integrated carbon, sulfur, and nitrogen isotope chemostratigraphy of the Ediacaran Lantian Formation in South China: spatial gradient, ocean redox oscillation, and fossil distribution. Geobiology 15, 552–571.
Wang, W., Zhou, C., Yuan, X., Chen, Z., Guan, C., 2011. Variations of the carbonate carbon isotope in Ediacaran Doushantuo ocean of South China. J. Stratigraphy 35, 349–360.
Wang, W., Zhou, C., Yuan, X., Chen, Z., Xiao, S., 2012. A pronounced negative $\delta^{13}C$ excursion in an Ediacaran succession of western Yangtze Platform: a possible equivalent to the Shuram event and its implication for chemostratigraphic correlation in South China. Gondwana Res. 22, 1091–1101.
Wang, X., Erdtmann, B.D., Chen, X., Mao, X., 1998. Integrated sequence-, bio- and chemostratigraphy of the Terminal Proterozoic to lowermost Cambrian "black rock series" from central South China. Episodes 21, 178–189.
Wang, X., Jiang, G., Shi, X., Xiao, S., 2016. Paired carbonate and organic carbon isotope variations of the Ediacaran Doushantuo Formation from an upper slope section at Siduping, South China. Precambr. Res. 273, 53–66.
Wang, Z., Wang, J., Suess, E., Wang, G., Chen, C., Xiao, S., 2017b. Silicified glendonites in the Ediacaran Doushantuo Formation (South China) and their potential paleoclimatic implications. Geology 45, 115–118.
Willman, S., Moczydłowska, M., 2008. Ediacaran acritarch biota from the Giles 1 drillhole, Officer Basin, Australia, and its potential for biostratigraphic correlation. Precambr. Res. 162, 498–530.
Xiao, S., Jiang, G., Ye, Q., Ouyang, Q., Banerjee, D.M., Singh, B.P., Muscente, A.D., Zhou, C., Hughes, N.C., 2022. Systematic paleontology, acritarch biostratigraphy, and $\delta^{13}C$ chemostratigraphy of the early Ediacaran Krol A Formation, Lesser Himalaya, northern India. J. Paleontol. https://doi.org/10.1017/jpa.2022.7.
Xiao, S., McFadden, K.A., Peek, S., Kaufman, A.J., Zhou, C., Jiang, G., Hu, J., 2012. Integrated chemostratigraphy of the Doushantuo Formation at the northern Xiaofenghe section (Yangtze Gorges, South China) and its implication for Ediacaran stratigraphic correlation and ocean redox models. Precambr. Res. 192–195, 125–141.
Xiao, S., Narbonne, G.M., 2020. The Ediacaran Period. In: Gradstein, F.M., Ogg, J.G., Schmitz, M.D., Ogg, G.M. (Eds.), Geologic Time Scale 2020. Elsevier, Amsterdam, pp. 521–561.
Xiao, S., Narbonne, G.M., Zhou, C., Laflamme, M., Grazhdankin, D.V., Moczydlowska-Vidal, M., Cui, H., 2016. Towards an Ediacaran time scale: problems, protocols, and prospects. Episodes 39, 540–555.
Xiao, S., Zhou, C., Liu, P., Wang, D., Yuan, X., 2014. Phosphatized acanthomorphic acritarchs and related microfossils from the Ediacaran Doushantuo Formation at Weng'an (South China) and their implications for biostratigraphic correlation. J. Paleontol. 88, 1–67.
Xue, Y., Tang, T., Yu, C., 1992. Discovery of the oldest skeletal fossils from upper Sinian Doushantuo Formation in Weng'an, Guizhou, and its significance. Acta Palaeontol. Sin. 31, 530–539.
Yin, C., Liu, P., Awramik, S.M., Chen, S., Tang, F., Gao, L., Wang, Z., Riedman, L.A., 2011a. Acanthomorph Biostratigraphic Succession of the Ediacaran Doushantuo Formation in the East Yangtze Gorges. South China. Acta Palaeontol. Sin. 85, 283–295.
Yin, L., 1987. Microbiotas of latest Precambrian sequences in China, in: Nanjing Institute of Geology and Palaeontology, Academia Sinica (Ed.), Stratigraphy and Palaeontology of Systemic Boundaries in China: Precambrian–Cambrian Boundary (1). Nanjing University Press, Nanjing, pp. 415–494.
Yin, L., Wang, D., Yuan, X., Zhou, C., 2011b. Diverse small spinose acritarchs from the Ediacaran Doushantuo Formation, South China. Palaeoworld 20, 279–289.
Yuan, X., Chen, Z., Xiao, S., Zhou, C., Hua, H., 2011. An early Ediacaran assemblage of macroscopic and morphologically differentiated eukaryotes. Nature 470, 390–393.
Zang, W., Walter, M.R., 1992. Late Proterozoic and Cambrian microfossils and biostratigraphy, Amadeus basin, central Australia. Association of Australasian Palaeontologists, Brisbane.
Zhang, Y., Yin, L., Xiao, S., Knoll, A.H., 1998. Permineralized fossils from the Terminal Proterozoic Doushantuo Formation, South China. J. Paleontol. 50, 1–52.
Zhou, C., Jiang, S., Xiao, S., Chen, Z., Yuan, X., 2012. Rare earth elements and carbon isotope geochemistry of the Doushantuo Formation in South China: implication for middle Ediacaran shallow marine redox conditions. Chin. Sci. Bull. 57, 1998–2006.

Zhou, C., Tucker, R., Xiao, S., Peng, Z., Yuan, X., Chen, Z., 2004. New constraints on the ages of Neoproterozoic glaciations in south China. Geology 32, 437–440.
Zhou, C., Xiao, S., 2007. Ediacaran $\delta^{13}C$ chemostratigraphy of South China. Chem. Geol. 237, 89–108.
Zhou, C., Xiao, S., Wang, W., Guan, C., Ouyang, Q., Chen, Z., 2017. The stratigraphic complexity of the middle Ediacaran carbon isotopic record in the Yangtze Gorges area, South China, and its implications for the age and chemostratigraphic significance of the Shuram excursion. Precambr. Res. 288, 23–38.
Zhou, C., Xie, G., McFadden, K.A., Xiao, S., Yuan, X., 2007. The diversification and extinction of Doushantuo-Pertatataka acritarchs in South China: causes and biostratigraphic significance. Geol. J. 42, 229–262.
Zhou, C., Yuan, X., Xiao, S., Chen, Z., Hua, H., 2019. Ediacaran integrative stratigraphy and timescale of China. Sci. China Earth Sci. 62, 7–24.
Zhu, M., Zhang, J., Yang, A., 2007. Integrated Ediacaran (Sinian) chronostratigraphy of South China. Palaeogeogr. Palaeoclimatol. Palaeoecol. 254, 7–61.